Role of Environmental Factors in Rapid Intensification and Weakening of Cyclone Ockhi (2017)

Jyothi Lingala[1], Sudheer Joseph[1], and Suneetha P[2]

[1]Indian National Centre for Ocean Information Services
[2]Andhra University,

November 28, 2022

Abstract

In this study, we investigate the oceanic and atmospheric processes that have contributed to the Rapid Intensification (RI) and Rapid Weakening (RW) of Cyclone Ockhi using the HYbrid Coordinate Ocean Model (HYCOM) simulations and Global Forecast System (GFS) outputs. The environmental conditions prevailed before RI showed the presence of thick warm and fresh waters, ample supply of mid-tropospheric relative humidity, and moderate wind shear. The intrusion of dry air, strong vertical wind shear, and unfavourable oceanic conditions annihilated the storm intensity during the RW stage. Compared to the ocean temperature, the vertical structure of salinity showed remarkable differences between the RI and RW locations resulting in contrasting upper-ocean stratification. The dynamic temperature (T$_{dy}$) under the TC core evolved under the influence of upper-ocean stratification showed a large drop at RW compared to RI. T$_{dy}$ provided a better representation of the ocean's negative feedback on the rapid intensity changes of TC Ockhi compared to TCHP, especially for the region like RI, which was primarily influenced by the salinity stratification. Hence, this study demonstrates the importance of multi-parameter metric like T$_{dy}$ in the assessment of oceanic feedback to TC and its intensity changes.

Role of Environmental Factors in Rapid Intensification and Weakening of Cyclone Ockhi (2017)

Lingala Jyothi[1,2], Sudheer Joseph[1], Suneetha P[2]

[1]Indian National Centre for Ocean Information Services, Hyderabad, Ministry of Earth Sciences, India
[2]Department of Meteorology and Oceanography, College of Science and Technology, Andhra University, Visakhapatnam, India

Key Points:

- The difference in the depth of mixing length and 26°C isotherm emphasize the importance of salinity stratification and storm parameters in modulating the ocean feedback to TC Ockhi.
- TC Ockhi induced dynamic temperature variations at the storm center are small during rapid intensification and large during rapid weakening.
- The strong (weak) upper ocean stratification together with the favorable (unfavorable) atmospheric conditions near the southeastern (northeastern) Arabain Sea, resulted in rapid intensification (rapid weakening) of TC Ockhi.

Corresponding author: Sudheer Joseph, sjo@incois.gov.in

Abstract

In this study, we investigate the oceanic and atmospheric processes that have contributed to the Rapid Intensification (RI) and Rapid Weakening (RW) of Cyclone Ockhi using the HYbrid Coordinate Ocean Model (HYCOM) simulations and Global Forecast System (GFS) outputs. The environmental conditions prevailed before RI showed the presence of thick warm and fresh waters, ample supply of mid-tropospheric relative humidity, and moderate wind shear. The intrusion of dry air, strong vertical wind shear, and unfavourable oceanic conditions annihilated the storm intensity during the RW stage. Compared to the ocean temperature, the vertical structure of salinity showed remarkable differences between the RI and RW locations resulting in contrasting upper-ocean stratification. The dynamic temperature (T_{dy}) under the TC core evolved under the influence of upper-ocean stratification showed a large drop at RW compared to RI. T_{dy} provided a better representation of the ocean's negative feedback on the rapid intensity changes of TC Ockhi compared to TCHP, especially for the region like RI, which was primarily influenced by the salinity stratification. Hence, this study demonstrates the importance of multi-parameter metric like T_{dy} in the assessment of oceanic feedback to TC and its intensity changes.

Plain Language Summary

Tropical Cyclones undergo intensity changes when they encounter favourable environmental conditions like the warm ocean, weak wind shear, and massive humidity. In this paper, we investigated the differences between those oceanic and atmospheric factors at the regions where rapid intensification (RI) and rapid weakening (RW) of Cyclone Ockhi took place. The analysis revealed that the waters are warm and fresh near the RI region and relatively cold and saline near the RW region. Although the thick warm ocean is a vital factor in modulating the TC intensity at RI, it was unclear to what depth the TC had interacted with the ocean and obtained its feedback. Besides, the magnitude of this feedback is a function of upper-ocean stratification, storm state, and speed. Hence, to account for all these parameters, we adopted a new ocean metric known as dynamic temperature to estimate the ocean's impact on TC intensity. The dynamic temperature at RI and RW regions showed remarkable differences due to strong contrast in salinity stratification.

1 Introduction

Cyclonic storms are one of the most destructive natural phenomena which result in human loss and property damage within a short period (K. Emanuel, 2003; Frank & Husain, 1971). With recent developments in scientific and technological spheres along with advances in satellite observations, the accuracy of track and intensity prediction of Tropical Cyclones (TCs) have shown significant improvements (Le Marshall et al., 2002; U. Mohanty et al., 2019). However, Rapid Intensification (RI) and Rapid Weakening (RW) storms make the prediction harder, even with the latest developments. RI (RW) is defined as an increase (decrease) of maximum sustained wind speeds by at least 30 kts (15.4 ms^{-1}) in 24 hours (Kaplan & DeMaria, 2003; Wood & Ritchie, 2015). Studies carried out by Bhatia et al. (2019) and K. Emanuel (2017) showed that there is ample evidence for increased occurrences of rapidly intensifying storms under the global warming scenario in the recent past. Thus, it is crucial to understand the processes associated with RI and RW phases of tropical storms for facing the challenges in TC track and intensity predictions that may arise in the future. The rapid growth/decay of a TC is typically associated with the non-linear interaction of many complicated mechanisms. These include, TC inner-core dynamics (such as inner-core asymmetry, eyewall replacement), upper-ocean interaction (such as ocean temperature, air-sea energy exchanges, sea spray) and atmospheric circulation (such as vertical wind shear and relative humidity) (Donelan et al., 2004; Gao et al., 2016; Holliday & Thompson, 1979; Kaplan et al., 2010; Lin et al., 2008; Marks et al., 1998; Montgomery et al., 2015; Schade & Emanuel, 1999; Y. Wang & Wu, 2004; Willoughby et al., 1982). Due to the multi-scale complex processes involved during these interactions, it is a challenging task to predict the TC intensity, especially the rapid changes (Elsberry, 2014; Krishnamurti et al., 2005).

Earlier studies have documented that large-scale environmental factors, in particular, warm ocean with a deep mixed layer, weak vertical wind shear (VWS) and high mid-tropospheric relative humidity (RH) may favour RI of a TC (Gray, 1968; Kaplan et al., 2010). The importance of warm sea surface temperature (SST) as a significant source of energy in maintaining the TC intensity is well-known (Bosart et al., 2000; Malkus & Riehl, 1960; Rotunno & Emanuel, 1987; Shay et al., 2000). Also, to account for the impact of the subsurface ocean on the TC's intensity, the ocean heat integrated from the surface to 26°C isotherm, known as Tropical Cyclone Heat Potential (TCHP) is being used (Goni et al., 2007; Leipper & Volgenau, 1972; Shay et al., 2000). However, TCHP has limitations in fully representing the role of upper-ocean stratification, which affects the vertical ocean mixing and further, the TC intensity (Balaguru et al., 2012; Jangir et al., 2016; Lin et al., 2009; Price et al., 2008). Another ocean parameter that has a significant impact on the storm intensity is the Barrier Layer (BL), defined as an intermediate layer between the base of the mixed layer and the base of the isothermal layer (Foltz & McPhaden, 2009; Sengupta et al., 2008; Sprintall & Tomczak, 1992). This layer limits the entrainment of deep colder waters into the relatively warm near-surface mixed layer and thus suppress the TC induced ocean cooling (Balaguru et al., 2012; Neetu et al., 2012). Recently, Balaguru et al. (2015) introduced a new ocean metric known as, TC dynamic temperature (T_{dy}) which better represents the impact of upper ocean conditions on the TC development. Unlike TCHP, where heat is integrated from surface to fixed isotherm, T_{dy} averages the temperature from surface to a variable mixing length. The computation of mixing length accounts for both temperature and salinity stratification (Balaguru et al., 2015) in estimating the TC induced ocean feedback.

Recently many studies on TC Ockhi described the causes for its rapid intensity changes (Singh et al., 2020), cyclogenesis and recurvature (Sanap et al., 2020), upper oceanic responses induced by the storm and its impact on the biological processes (Ganguly et al., 2020; Lü et al., 2020). Based on satellite and reanalysis datasets, Singh et al. (2020) and Sanap et al. (2020) explained the importance of warm oceanic temperatures over the southeast Arabian Sea (SEAS) in the rapid development of TC Ockhi. However, none of those studies explored the role of salinity and its relation to the intensity evolution of TC Ockhi. Hence, in this paper, we chose to have a detailed analysis of the processes in the ocean and atmosphere associated with the RI and RW phases of TC Ockhi. The objective of this study is accomplished with the help of outputs from General Circulation Models with high spatial and temporal resolution. We organized the rest of the paper as follows. Section 2 describes the details of the model and observational data sets used for the analysis. Section 3 gives an overview of TC Ockhi. The verification of vertical temperature and salinity is available in Section 4. Section 5 discusses the preexisted oceanic and atmospheric conditions before RI and RW that has led to rapid intensity changes. Later, this section discusses the significant differences in the negative SST feedback along the storm track. Furthermore, it explains the role of the environmental factors in regulating this feedback. Section 6 presents a discussion and summary of the results of this study.

2 Data and Methods

To conduct this study, we used ocean parameters (temperature, salinity, u and v currents) from HYbrid Coordinate Ocean Model (HYCOM) and atmospheric parameters (heat fluxes, wind, RH) from Global Forecast System (GFS). We obtained the ocean parameters from a 1/16° resolution model for the Indian Ocean domain (20°E - 120°E, 43.5°S - 30°N) at three-hourly intervals for the cyclone period. The model run is initialized on 2^{nd} March 2017 using a restart file obtained from the operational setup at Indian National Centre for Ocean Information Services (INCOIS) with data assimilation. However, we did not perform data assimilation from March to December 2017 run. The bias-corrected GFS three-hourly atmospheric heat flux, precipitation, and momentum flux along with river discharge from Naval Research Laboratory (NRL) climatology are used to force the model. Model bathymetry used is a combination of the General Bathymetric Chart of the Oceans (GEBCO) and ETOPO-1. We used the K-Profile Parameterization (KPP) mixing scheme. A detailed validation and other specifics about HYCOM can be found in the technical report `https://incois.gov.in/documents/TechnicalReports/ESSO-INCOIS-CSG-TR-01-2018.pdf`. The wind and RH data having a 0.5° spatial resolution and three-hourly temporal resolution at different atmospheric levels (10m, 850 hPa, 700 hPa, 200 hPa) are used to compute wind speed, shear, and mid-tropospheric humidity. Track related information such as storm position, intensity, and translation speed at a six-hourly interval is obtained from the Indian Meteorological Department (IMD) Best Track data (`http://www.rsmcnewdelhi.imd.gov.in/index.php?option=com_content&view=article&id=48&Itemid=194&lang=en`). The translation speed of the storm is obtained from the International Best Track Archive for Climate Stewardship (IBTrACS). The monthly mean vertical profiles of temperature and salinity are obtained from EN4 (`http://www.metoffice.gov.uk/hadobs/en4/index.html`) for the year 2017 and are used to verify the HYCOM simulations. In this study, VWS is calculated by taking the difference of wind vectors at 850 hPa and 200 hPa levels (Kotal et al., 2014; Park et al., 2012). The mid-tropospheric humidity is computed by taking the average of RH between the 850 hPa and 700 hPa levels (Kaplan & DeMaria, 2003). The term TCHP is computed using the HYCOM temperature following the below equation (Leipper & Volgenau, 1972):

$$TCHP = \int_{z_0}^{z_{26}} \rho C_p (T(z) - 26) dz$$

ρ is the seawater density, C_p is the specific heat at constant pressure, T(z) is the temperature at dz level, z_{26} is the depth corresponding to 26°C isotherm. The term Barrier Layer Thickness (BLT) is taken as the difference between Isothermal Layer Depth (ILD) and Mixed Layer Depth (MLD). ILD is defined as the depth at which the temperature is 0.2°C lower than the SST (Kara et al., 2003). MLD is defined as the depth at which the density increases by $0.05kg/m^3$ compared to the surface value (Chaudhuri et al., 2019). T_{dy} is computed following Balaguru et al. (2015) and is defined as:

$$T_{dy} = \frac{1}{L} \int_0^L T(z) dz$$

T_{dy} is the vertical averaged temperature from the surface to the variable mixing length (L), T(z) is the temperature at z depth. L is calculated as follows:

$$L = h + \left(\frac{2\rho_0 u_*^3 t}{\kappa g \alpha} \right)$$

where, h is the initial MLD, ρ_0 is the seawater density, u_* is the friction velocity, t is the average time of mixing under the storm, κ is the von Karman constant, g is the acceleration due to gravity, α is the rate of increase of potential density with depth beneath the mixed layer.

3 Overview of Cyclone Ockhi

A Very Severe Cyclonic Storm (VSCS) christened as Ockhi originated over the south-western part of the Bay of Bengal (BoB) on 29^{th} November 2017. It is considered the most powerful storm in the AS since Cyclone Megh in 2015 to impact the coastal population around the southern part of India. The track and intensity category of the storm are shown in Figure 1a. TC Ockhi developed rapidly from Deep Depression (DD) (29^{th} November 2017) to Cyclonic Storm (CS) (30^{th} November 2017) within six hours, as it skirted the tip of the Indian coastal shelf of about 200m depth (bathymetry is not shown). Due to its proximity to the coastal population, severe damage has occurred to the southern part of India (Singh et al., 2020). In the next few hours, it moved north-westward and rapidly intensified from the category CS to VSCS near the southeastern part of the AS. The favourable oceanic and atmospheric conditions across this region are detailed in the later section. Although TC Ockhi intensified rapidly in the initial stages, it rapidly weakened near the coast of Gujarat from 4^{th} December 2017 before making landfall. In the rest of the paper, we refer to the RI stage as 1^{st} December 00hrs to 2^{nd} December 00hrs, while the RW stage as 4^{th} December 09hrs to 5^{th} December 09hrs.

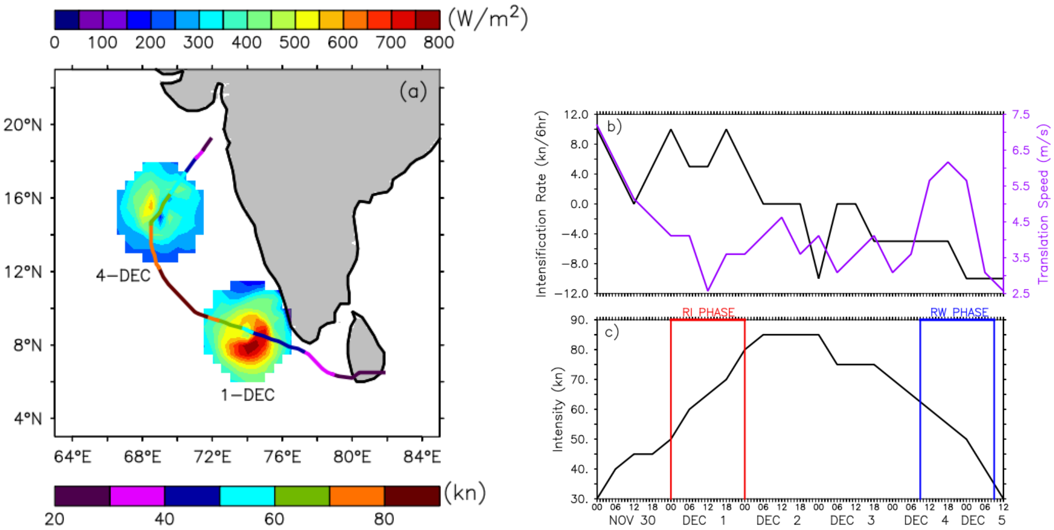

Figure 1. a) Snapshots of enthalpy fluxes (shaded) on 1^{st} and 4^{th} December 2017, overlaid by track and intensity of TC Ockhi. b) The observed rate of intensification (black) and translation speed (purple) of TC. c) Intensity of TC in terms of maximum sustained wind speed during November 30^{th} - December 5^{th} 2017. The RI and RW phases are indicated by red and blue colors respectively in c).

The significance of enthalpy fluxes in the development and maintenance of the TCs is well known as they are the major source of energy (K. A. Emanuel, 1986; Guinn & Schubert, 1993; Miller, 1958; Ooyama, 1969; Shay et al., 2000). Past studies on storm cases like Hurricane Earl and TC Nargis have reported that there was an increase in enthalpy fluxes during the peak intensity stage where the warm ocean caused a weak negative SST feedback (Jaimes et al., 2015; Lin et al., 2009). Figure 1a depicts the enhanced ($\sim 800\ W/m^2$) enthalpy fluxes (latent+sensible) during RI (1^{st} December) and weakened ($\sim 300\ W/m^2$) fluxes during RW (4^{th} December) for the region sampled around the storm center. In the later sections, we try to examine the impact of the underlying oceanic state during RI and RW stages on the varying magnitude of enthalpy fluxes. The dependence of TC intensification on the translation speed is widely discussed in the literature (Chang et al., 2020; Lin et al., 2009; Mei et al., 2012; Y. Wang & Wu, 2004). Their studies showed that the fast (slow) moving storms tend to induce lesser (larger) ocean cooling due to the decreased residence time over the ocean. Resulting differences in the magnitude of the negative SST feedback to the TC, in turn, has a significant impact on its intensity. Figure 1b shows the along-track intensification rate (black curve) plotted against the translation speed (purple curve). Figure 1c displays the intensity of TC Ockhi in terms of maximum sustained wind speed. The RI and RW phases are indicated by red and blue lines in Figure 1c. As seen in Figure 1b the rate of intensification is larger (10kts/6hr) during the RI stage (1^{st} December 00hrs to 2^{nd}December 00hrs) and lesser (-6 kts/6hr) during the RW stage (4 th December 00hrs to 5^{th} December 09hrs). It is also evident that the translation speed is relatively slower (≈2.5 - 3.5m/s) during RI and faster (≈6.5 m/s) during RW stages. Many of the existing literature (Mei et al., 2012; Zedler, 2009) showed that there is a one-to-one relation between translation speed and intensity. However, in the case of TC Ockhi, the relationship is inverse during RI and RW stages, which is intriguing. Lin et al. (2009), noted that the inverse association might also exist as long as the ocean has deep enough warm waters to counter the TC-induced cooling while moving slowly. Therefore, we examined the role of the upper ocean on the TC intensity and the TC-induced ocean cooling in section 5.5.

4 Verification of Model Temperature and Salinity

To evaluate the ocean model performance, we compared the vertical profiles of HYCOM temperature and salinity against the EN4 data between 5-150m depth, as shown in Figure 2a-f. We extracted the model and EN4 data from 2° box region centred at RI location. Figure 2 shows the model temperature profiles (Figure 2b) agrees well with the observed temperature (Figure 2a). The averaged temperatures across the sampled region show intense warming (> 28°C) from March to May reaching up to a depth of ≈ 50m in both model and observations. During August through September, there is a shoaling of isotherms both in the model and EN4 data resulting in subsurface cooling of nearly 2°C. Further, there is a slow deepening of 26°C isotherms, causing the build-up of thick warm waters from October. By the end of November, i.e., before the arrival of TC Ockhi this region became conducive for the TC development with the warm ocean and deeper 26°C isotherm extending up to ≈50m depth.

The model salinity profiles (Figure 2e) shows a reasonably good match with the observed profiles (Figure 2d) in the sampled region. The vertical structure shows the presence of low saline waters in the surface layers that started appearing in November and December, and its existence became more prominent during January and February months. Past studies by (Kumar & Mathew, 1997; Nyadjro et al., 2012) showed that low saline water is intruded from the BoB basin and is associated with the development of BL in this region. The high-resolution model data is interpolated on to EN4 data which is 1° and monthly average. Hence, the presence of low saline water during November and December months is not projected clearly in the model data. This feature will be shown in detail in sections 5.1 and 5.3. The surface salinity increased from June and sustained till October month, with a subsurface maximum. Although the model captures the salinity pattern, the amplitude is underestimated by nearly 0.5PSU. The correlation of the vertical profiles of temperature and salinity are computed and shown in Figure 2c and Figure 2f respectively. The correlation values of temperature profiles are above 0.9 from the surface to 150m depth which is significant at 99%. Similarly, the correlation between model and EN4 salinity showed a good match up to ≈70m depth and decreased in the range of 70-95m. Although there is a poor correlation in the subsurface, we are mainly focussing on near-surface salinity variability in this study. However, the minor issues with the magnitude of HYCOM temperature and salinity simulations may not affect our objectives as the pattern of the major features are in good match with those observed.

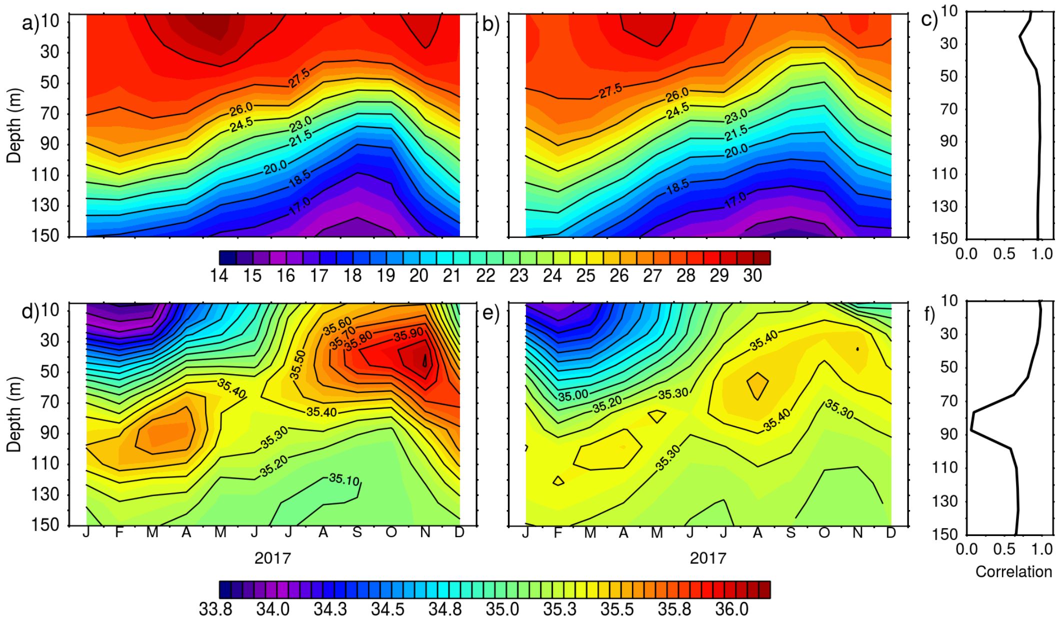

Figure 2. Comparison of a) EN4 temperature with the b) HYCOM simulations during January through December 2017. Similarly, d) and e) indicate salinity profiles. c) and f) show the correlation between EN4 and HYCOM for temperature and salinity profiles.

5 Results

5.1 Ocean and atmospheric conditions before RI and RW

Earlier studies have shown significant differences in the environmental factors between RI and non-RI TC cases (Kaplan et al., 2010; Kaplan & DeMaria, 2003; Molinari & Vollaro, 2010). Unlike past studies that have compared the TC environments between different storm cases here, we considered a single storm that had undergone both RI and RW phases during its lifetime. We evaluated the spatial patterns of ocean fields from HYCOM, and atmospheric variables from GFS prevailed before the RI and RW stages of TC Ockhi. In the rest of the paper, the pre-existed conditions of RI refer to the environmental conditions on 28th November 00hrs, as TC Ockhi started intensifying from 1st December 00hrs till 2nd December 00hrs over SEAS. Similarly, the pre-conditions of the RW phase refer to 1st December 09hrs as TC Ockhi started weakening from 4th December 09 hrs till 5th December 09 hrs over the northeastern AS (NEAS). Figure 3 shows the snapshots of pre-existed conditions of SST, salinity, VWS, and RH before the RI (on 28th November) and RW (on 1st December) phases of TC Ockhi. The 24hrs duration of RI (Figure 3a,c,e,g) and RW (Figure 3b,d,f,h) phases are marked by cyclone symbols.

As shown in Figure 3a, two days before the occurrence of RI, the SEAS had warm ($\approx 30°$C) waters, especially along the path of TC where it had intensified rapidly. Previous studies have shown that during October-November months, the SSTs in the SEAS are relatively warmer (28.5°C) (Luis & Kawamura, 2003; Srinivas & Kumar, 2006) and reach peak values (30°C) before the onset of monsoon (Shenoi et al., 2005). Fundamentally, the TC intensity is a function of warmer SSTs as they trigger the rate of evaporation at the air-sea interface (K. A. Emanuel, 1986). Together with the warmer SSTs, the SEAS is characterized by low saline ($\sim$ 33 PSU) waters, as shown in Figure 3c. During October through December months, the East India Coastal Current (EICC) pumps the low saline waters from the BoB basin along the coast of India and Sri Lanka. The freshwater input into the SEAS enhances the formation of BLT (Shenoi et al., 2005), which plays a crucial role in governing the TC intensity. Therefore, the advection of low saline waters and warm SSTs formed a conducive environment over SEAS for the TC development however they aren't sufficient conditions. On the other hand, Figure 3b&d shows relatively cooler ($\sim 27°$C), and high saline (36.5 PSU) waters persisting before the RW phase, i.e., on 1^{st} December 09 hrs over the NEAS.

While considering atmospheric parameters, VWS is an important dynamical parameter associated with the development and intensification of TC. Earlier studies have demonstrated the impact of strong VWS on the ventilation of heat and moisture fluxes away from the storm center, and in turn, its impact on the TC intensity (DeMaria, 1996; Gray, 1968; Riehl & Shafer, 1944; Wong & Chan, 2004). The typical range of wind shear values that favor the TC development is 5 - 10kt (2.5 - 5 ms^{-1}) classified as weak shear; 10 - 20kt (5 - 10 ms^{-1}) known as moderate shear, which forms an unfavorable (neutral) environment for weak (mature) storms; above 20 kt (10 ms^{-1}) is considered as strong shear which favors the RW (U. C. Mohanty & Gopalakrishnan, 2016). Figure 3e-h demonstrates the atmospheric conditions prevailed before the occurrence of RI and RW phases. The differences between the distribution of VWS existed ahead of the RI and RW stages are depicted in Figure 3e&f, respectively. The cyclogenesis and development in the AS basin were mainly in the regions with shear values ranging from 5 - 10 ms^{-1} (Evan & Camargo, 2011). It is evident from Figure 3e that before the RI phase of TC Ockhi, the shear values are weak enough (< 10 ms^{-1}) to support the TC intensification over the SEAS; while Figure 3f shows the strong shear (> 10 ms^{-1}) conditions prevailed before the RW stage in the NEAS. Therefore, TC Ockhi has the range of favourable shear values before the RI stage, which is in line with the climatological study by Evan and Camargo (2011).

Besides VWS another crucial atmospheric factor that discriminates the intensifying storm from the non-intensifying storm is the moisture in the mid-troposphere (Komaromi, 2013; Smith & Montgomery, 2012). The sensitivity of TC size and intensity to the intrusion of dry air ($<$ 30% RH) into the TC core is well-documented (Hill & Lackmann, 2009; Kotal & Roy Bhowmik, 2013; Tang & Emanuel, 2010). Their studies concluded that the ample supply of moisture in the mid-troposphere favours the TC intensification. There are notable differences in the availability of mid-tropospheric humidity (%) before the RI and RW phases of TC Ockhi respectively (Figure 3g&h). The humidity in SEAS was very high (>90%) where the storm rapidly intensified (Figure 3g) and was very low (<30%) in NEAS where the RW took place (Figure 3h). The lower humidity values are associated with the evolution of dry air intrusion into the TC core which will be detailed in later section 5.1.1. Previous studies (Komaromi, 2013; Smith & Montgomery, 2012) showed that such low levels of saturation hinder the TC development. Thus, atmospheric conditions existed in SEAS catalyzed the intensification of TC Ockhi along with oceanic conditions.

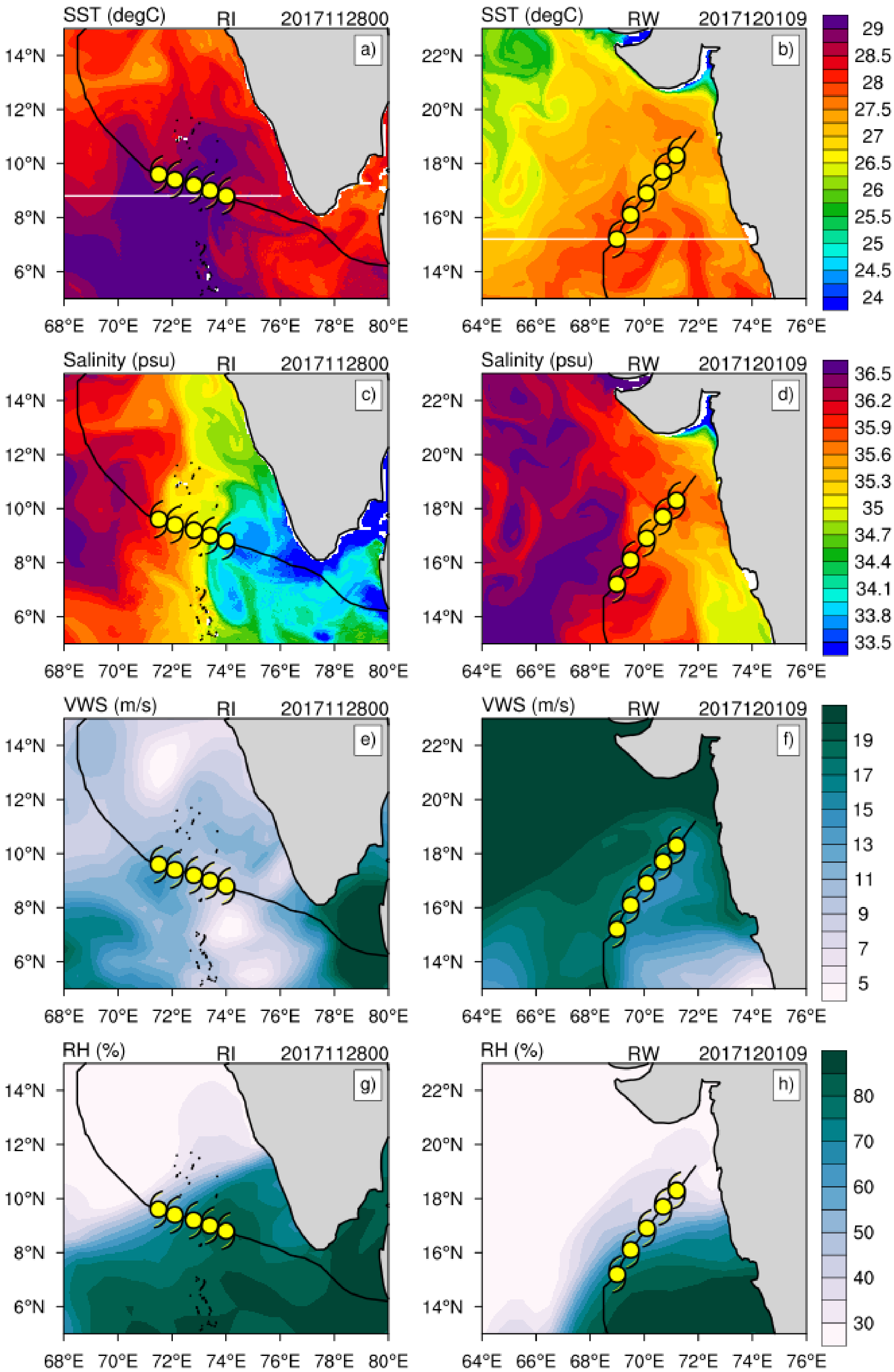

Figure 3. Spatial structure of preexisted a) SST c) Salinity e) VWS and g) RH before the RI stage (on 28^{th} November 00hrs). Similarly, b), d), f) and h) before the RW stage (1^{st} December 09hrs). White lines in a) and b) indicates the longitudinal sections at 8.8°N and 15.2°N which will be referred in section 5.3

5.1.1 Intrusion of dry air into the TC center during RW stage

Apart from ocean conditions, we have examined the intrusion of dry air into the core of the TC, which is widely recognized as a decaying factor for TC intensification. Past studies have highlighted the impact of dry air intrusion on the TC intensity, and its further development (Nolan, 2006; Simpson et al., 1958). There are many earlier TC cases (Onil (2004), Agni (2004), Gonu (2007), Nanauk (2014), Hikaa (2019)) in the AS basin which had dissipated before making landfall due to the lack of environmental moisture in the mid-troposphere. Another such case is TC Ockhi, which encountered dry air from 3^{rd} December and finally went through the RW phase from 4^{th} - 5^{th} December 2017. The snapshots of mid-tropospheric RH (shaded) overlaid by wind shear vectors (Figure 4) on selected dates depicts the intrusion of dry air into the TC inner core during its weakening phase. The vortex center in each plot represents the location of the TC core on respective dates. The larger values of RH (>95%) are extending up to 300km from the TC center on 3^{rd} December 00hrs and the organization looks symmetric during this time. In the next 12hrs, the symmetry of 95% humidity contour is disturbed, and the lower RH values started occupying the western sector of the TC. The replacement of moist air with the dry air continued during the next 24 hours, i.e., till 5^{th} December 12hrs, and by this time the system got disorganized completely. Hence, the intrusion of dry air has disturbed the symmetrical convection pattern around the TC center and favoured the RW phase in the northern AS. This observation is in agreement with the past studies (Kimball, 2006; Wu et al., 2015). Thus, apart from supportive oceanic conditions that weakened the storm, the distribution of humidity also played a vital role in its decay before it made landfall. As past research suggests the intensification/weakening of a TC is not an independent process, instead it is a non-linear interaction of several processes at various spatial and temporal scales.

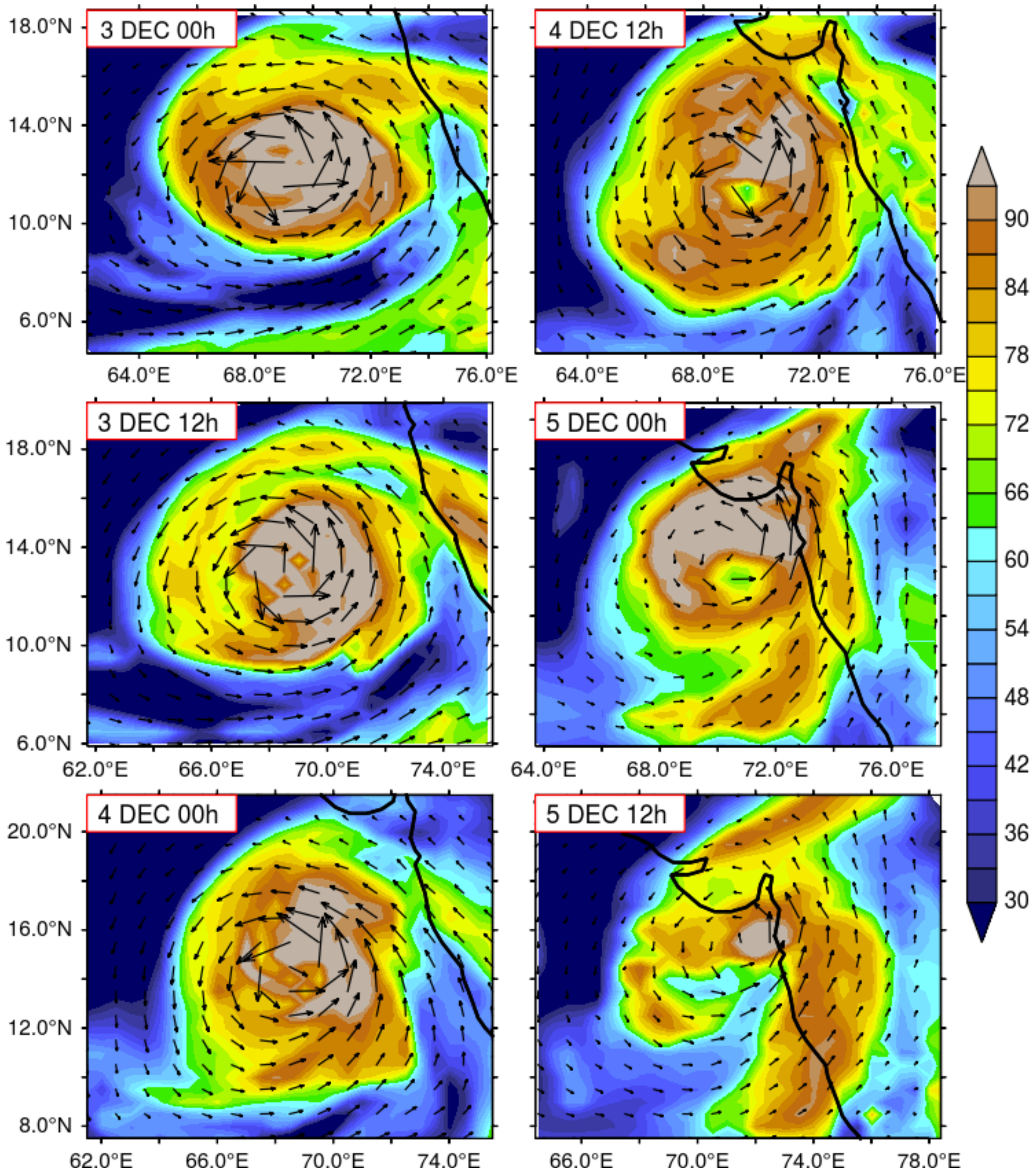

Figure 4. Snapshots of RH (%) overlaid by wind shear vectors on selected dates during 3^{rd} December 00hrs to 5^{th} December 12hrs.

5.2 SST anomaly in the 0.5° radius around the cyclone centre

Earlier studies (Bender et al., 1993; Dare & McBride, 2011; Price, 1981) have emphasized the impact of negative SST feedback due to the storm-induced ocean cooling on the development of TC. A significant drop in SST reduces the energy supply from the ocean to the TC, and thus SST acts as an essential factor for the TC intensity changes (Jacob et al., 2000; Shay et al., 1992). However, the magnitude of the TC-induced surface cooling is a function of TC intensity, translation speed, and the ocean mixed layer depth. The enormous surface wind stress generated by a propagating storm deepens the oceanic mixed layer through the process of turbulent mixing which lowers the SST (Brand, 1971; Price, 1981; Vincent et al., 2012). Slower (faster) moving storms tend to induce more (less) surface cooling, as they impart more (less) momentum into the ocean due to the longer (shorter) residence time (Dare & McBride, 2011; Lin et al., 2009; Mei et al., 2012). In the present section, we analyze the differences in the magnitude of SST anomalies (SSTA) recorded along the track of TC Ockhi from 30th November to 5th December.

SSTA is computed as the difference between SST after two days of storm passage, and SST averaged -12 to -2 days before the storm at a given location (Lloyd & Vecchi, 2011). Figure 5 shows the spatial SSTA variability influenced by the storm sampled over a 0.5° radius from the storm center. The magnitude of storm-induced cooling was limited on 30th November and 1st December, which coincides with the existence of warmer and fresher waters. As the storm propagated further northwest, there was a noticeable cooling found on 2nd December. The cooling was intense on this day and reached the peak value as it exited from the region of warm and fresh waters (Figure 3). Later, the amplitude of cooling reduced from 3rd December through 5th December, where the underlying oceanic state is relatively cooler and saline compared to SEAS. However, in agreement with the previous studies (Monaldo et al., 1997; Price, 1981; Stramma et al., 1986) the rightward bias of cooling was evident at all the sampled regions from 30th November - 5th December.

The box-plot of along-track SSTA variability sampled over a 0.5° radius (Figure 5b) from the storm centers shown in Figure 5a. SSTA on 30th November (0.01°C) and 1st December (0.2°C) showed positive anomalies compared to the negative anomalies during 2nd to 5th December. The warm anomalies provided positive SST feedback to the TC and favoured the RI in the next 24 hours. The maximum cooling on 30th November and 1st December is restricted to -0.3°C and -0.8°C respectively. The higher cooling (-2.8°C) observed on 2nd December is also probably due to the larger wind forcing (85 kn) imparted over the ocean. The minimum and maximum values ranged from -0.8°C and -2.8°C on 2nd December, in the TC core region. TC Ockhi started weakening from 2nd December which is in agreement with the past studies that have shown the sensitivity of TC intensity to the subtle variations in the inner core SST (Cione & Uhlhorn, 2003; Schade & Emanuel, 1999). The maximum SST cooling on 4th December is $\approx$ -1.4°C near the TC core region, and from thereon TC Ockhi underwent RW. Despite the slower translation speed on 1st December, TC Ockhi induced minimum SST cooling, which implies that the magnitude of cooling is also a function of other underlying oceanic conditions.

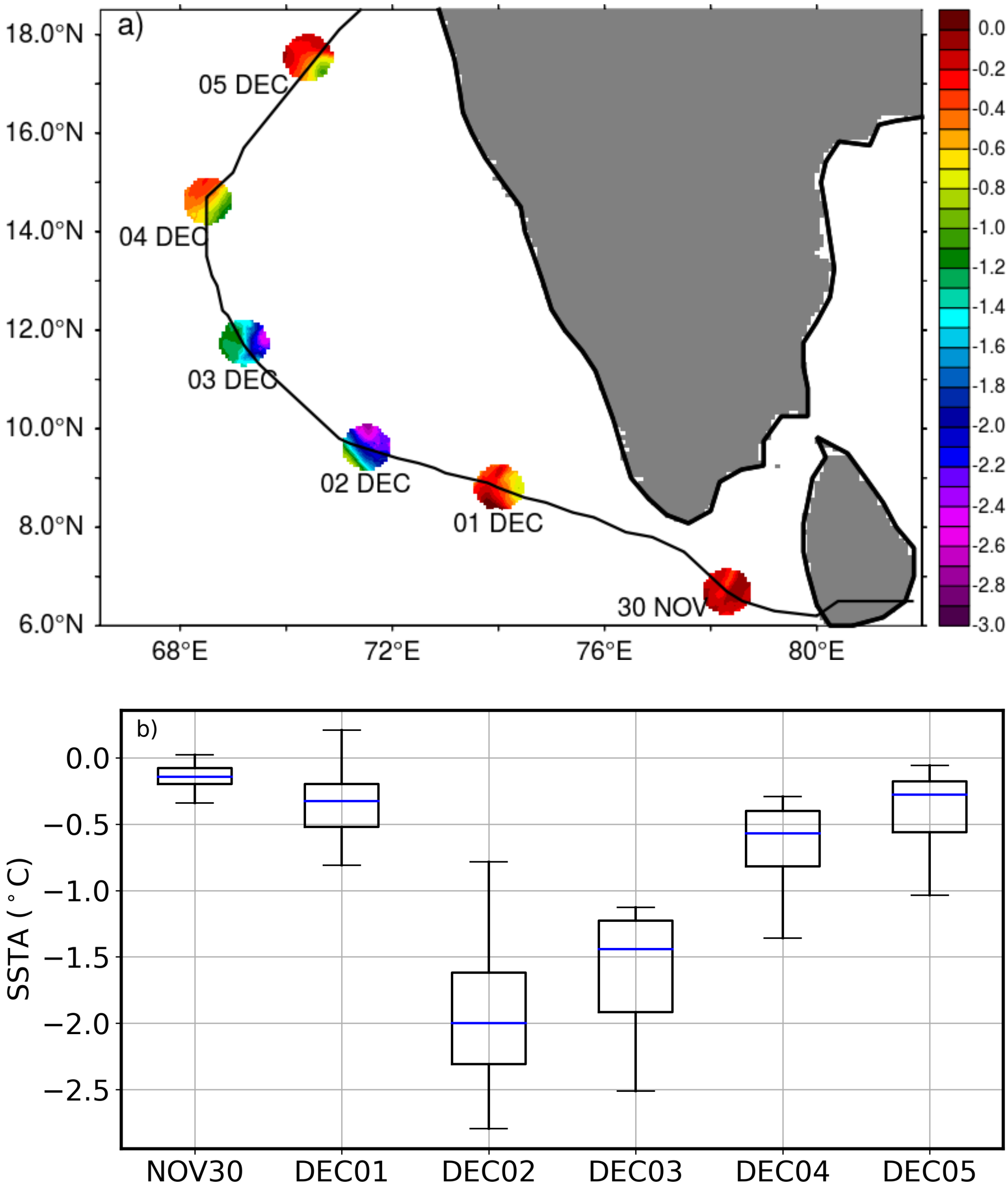

Figure 5. a) Spatial pattern of SSTA along the track of TC Ockhi during 30th November - 5th December 2017 sampled over 0.5° radius from the storm center. b) Boxplot of the sampled SSTA (°C) values in the circle shown in a)

5.3 Longitudinal sections of temperature and salinity

As the subsurface ocean is equally important as the surface ocean in modulating the TC intensity, we have also examined the vertical structure of temperature and salinity that prevailed before the RI and RW phases. Figure 6 shows the HYCOM derived vertical profiles of temperature and salinity from two longitudinal sections as marked (white lines) in Figure 3a&b. The first section is taken over the SEAS at 8.8°N (Figure 6a&c), and the second section is taken in the NEAS at 15.2°N (Figure 6b&d). We have selected these two latitudes, as the RI and RW phases initiated at these latitudes. The vertical sections of temperature and salinity at 8.8°N (15.2°N) are considered on 28th November (1st December). The location of the TC is marked by cyclone symbols (Figure 6).

The vertical structure of temperature from the SEAS (8.8°N) (Figure 6a&c) depicts the presence of warm waters ($>$ 29°C) from the surface to $\sim$20 m depth within the longitudinal range of 69°E - 74°E. Interestingly, the isotherms were deeper at the location were RI took place later (cyclone symbol) with 26°C isotherm reaching up to $\sim$80 m. Past studies related the depth of 26°C isotherm with the amount of heat stored in the subsurface and its critical role in fueling the TC heat engine (Shay et al., 2000). The salinity structure at 8.8°N is presented in Figure 6c. Consistent with Figure 3c, low salinity values (<34PSU) are observed in the band of 73.5°E - 76°E. As mentioned in section 5.1, the decrease in surface salinity is primarily due to the intrusion of freshwater brought by coastal boundary current which enhanced the salinity stratification up to $\sim$50m depth. Temperature profiles at 15°N (Figure 6b), reveals that the surface waters are relatively cooler ($\sim$ 27°C) than the southern section, and the depth of 26°C isotherm is shallower ($\sim$60m) than the former case. In contrast to the existence of fresher waters at 8.8°N, the high saline (36 PSU) values at 15°N. Therefore, as evident from Figure 3 and Figure 6 the RI location had thick warm, and fresher waters supporting TC intensification compared to the RW location. Apart from temperature and salinity, we have also investigated the conventional ocean metrics such as BLT and TCHP at RI and RW locations.

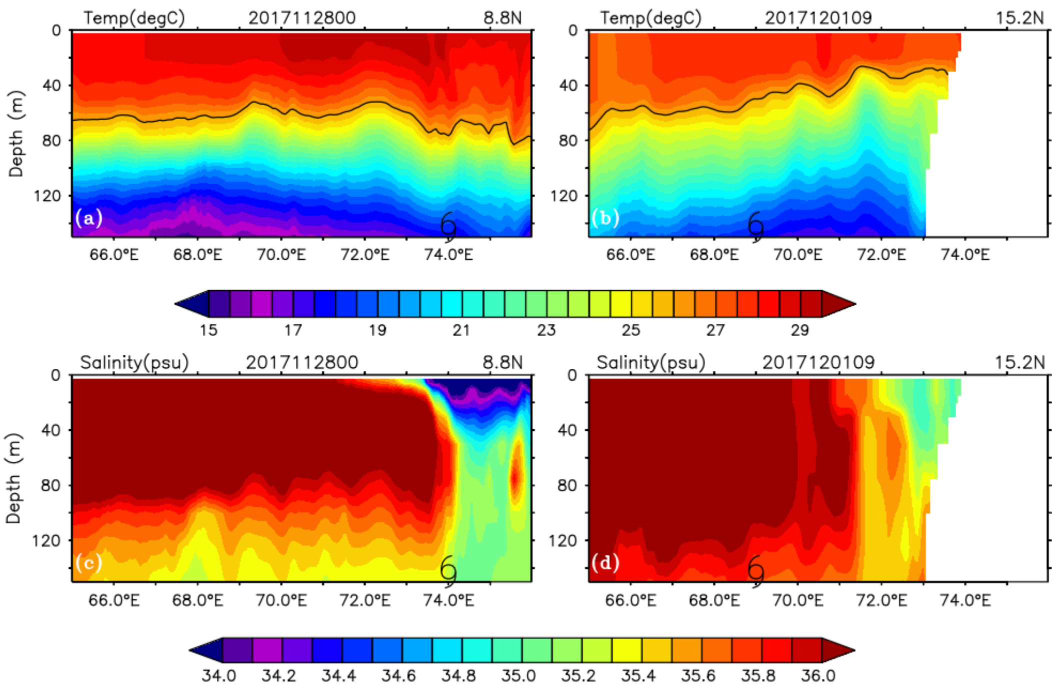

Figure 6. Vertical structure of temperature (a and b) and salinity (c and d) before the RI and RW phases at latitudes 8.8°N and 15.2°N respectively.

5.4 TCHP and BLT during RI and RW stages

The interaction of TC is not confined to the warm surface ocean alone; instead, it interacts with the subsurface as well (K. A. Emanuel, 1986). Hence, the importance of TCHP is widely discussed as it amplifies the storm intensity by nullifying the TC induced SST cooling (Ali et al., 2012; Goni & Trinanes, 2003; Lin et al., 2012; Shay & Brewster, 2010). For example, past cyclone cases in the north Indian Ocean such as Nargis (2008), Sidr (2010), and Viyaru (2013) had shown rapid intensity changes after encountering the regions of larger values of TCHP (Lin et al., 2012; Kashem et al., 2019). Although several studies documented the strong relationship between the TC intensity and warm SST (DeMaria, 1996; Evans, 1993; Sun et al., 2017), the upper ocean thermal energy measured up to a considerable depth acted as a more sensitive parameter in predicting the track and intensity changes than SST alone (Goni et al., 2007). Figure 7 illustrates the comparison of TCHP distribution among the RI and RW stages of TC Ockhi. The SEAS have higher values of TCHP off the coast, which increased towards the west as evident from Figure 7a. The values exceeding the threshold, 60 kJ/cm^2 (Mainelli et al., 2008) are coinciding with the RI stage, indicated by the TC symbol in Figure 7a. It is interesting to find the water with high TCHP is transported under the influence of a clockwise rotating eddy advecting water from the southern tip of India ($\sim$ 77°E) towards the RI location ($\sim$ 74°E).

From 20th November, a thick layer of warmer water brought by the ocean currents existed at the vicinity of TC track supporting high TCHP values (Figure 7b). A notable decrease of TCHP associated with shoaling of 26°C isotherm is observed in the RI region after the passage of TC. The impact of TC on the TCHP amplitude at the RI region is reflected up to 10th December, and later the TCHP started recovering to the prestorm state (Figure 7b). Figure 7c shows that the TCHP values near the RW location are nearly 30 kJ/cm^2, which are very less than the threshold value to support the energy supply for the TC sustenance. Also, from Figure 7d, it is evident that there was no existence of TCHP values above the threshold from 20th November through 14th December.

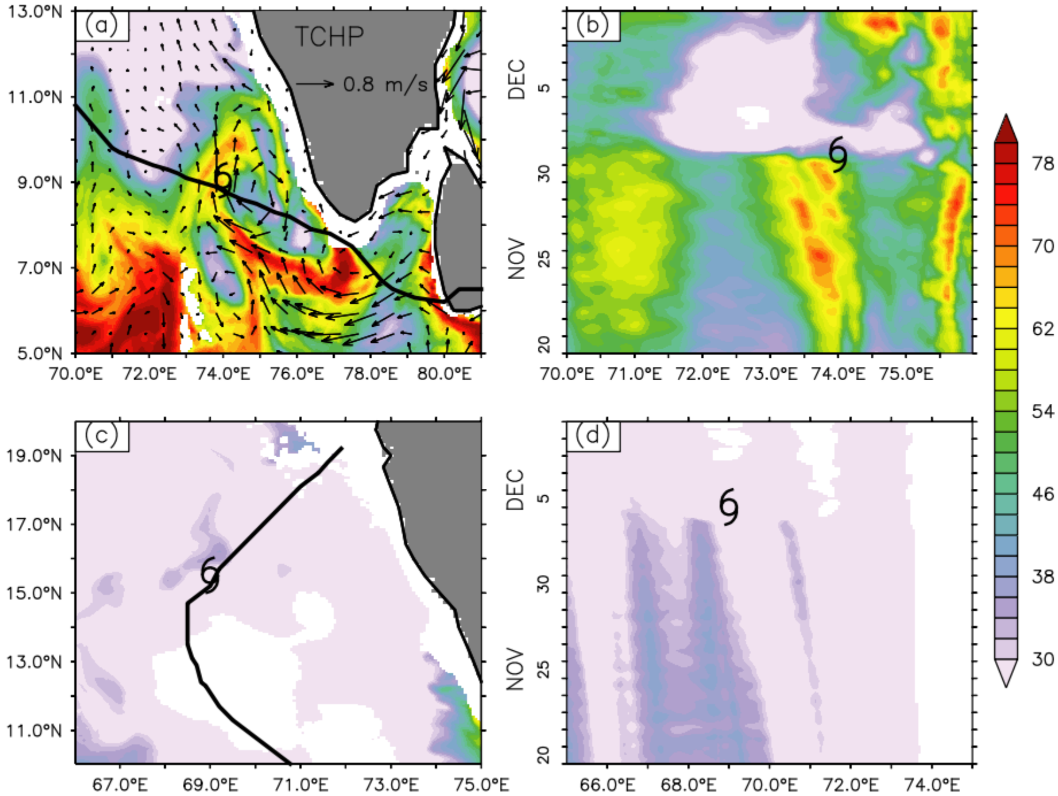

Figure 7. a) & c) Spatial distribution of TCHP (kJ/cm^2) during RI and RW stages respectively. Snapshots are taken on 1^{st} December for RI and 4^{th} December for RW periods. b) & d) Hovmoller plot of TCHP at latitude 8.8°N and 15.2°N, indicating RI and RW latitudes respectively. The position of the storm is represented by the cyclone symbol in all the plots. The overlaid vectors in a) represent the current vectors averaged for one week before 1^{st} December.

A study by Lin et al. (2009) reported that a TC could intensify even after encountering the shallow warm ocean characterized by $\sim$ 65-70 kJ/cm^2 of heat content, provided the storm speed is in the range $\sim$7 - 8 ms^{-1}. Similarly, a slow-moving storm ($\sim$2 - 3 ms^{-1}) intensifies over the ocean with warm and deeper mixed layer overcoming the TC induced negative SST feedback. Later, Jangir et al. (2016), analyzed the correlation between TC intensity and TCHP by examining 27 storm cases in the north Indian Ocean during 2005-2012. Their study revealed that more than 60% of the storms showed a negative correlation between the two parameters and TCHP could not be a sole predictor for the TC intensity change. In general, TCHP is measured up to the depth of 26°C isotherm, assuming that a TC cannot sustain at below temperatures (Byers, 1959). However, the depth of TC interaction with the ocean depends significantly on the prevailing oceanic state and the speed of the TC. TCHP does not account for the above parameters (Balaguru et al., 2015; Price et al., 2008) and hence may not reflect the ocean feedback properly in all cases.

Analysis carried out by (Balaguru et al., 2012; X. Wang et al., 2011) showed that BLT plays a significant role in the TC induced ocean mixing and further influences the TC intensity. The rate of intensification is $\sim$ 50% higher for a TC passing over a BL region when compared to the normal ocean (Balaguru et al., 2012). A thick BL existed in the SEAS near the southern tip of India and off the coast (Figure 8a). Thus, along with high TCHP values, the RI location (74°E) is also characterized by thick BL enhancing the potential for TC intensification. The BL formation at SEAS is related to the freshwater intrusion through the coastal boundary current from the BoB (Figure 3). The track of TC Ockhi encountered thick BL triggering the RI phase from the same region. Figure 8b show the BL structure from 20^{th} November through 14^{th} December at 8.8°N. After the passage of TC, on 1^{st} December, the BL is eroded due to the strong TC winds and thickness reduced to below 10 m. The impact of TC existed till 4^{th} December, and later the formation of BL is reinitialized with the aid of EICC. Figure 8c shows the spatial distribution of BL near the RW region. Even though high BLT values have existed in RW location, the translation speed of TC Ockhi at this time was 6 ms^{-1} (relatively fast-moving) therefore the TC did not get enough time to interact with the ocean.

Yan et al. (2017) showed that the relation between TC intensity and thickness of BL is much more complex than illustrated in the previous studies and argued that it is sensitive to the factors like the intensity of the storm, duration of the wind forcing, and upper-ocean stratification. Their study demonstrated that the presence of BL might either suppress or favour the TC growth depending on whether the TC wind forcing can break through the mixed layer base or the BL base. Therefore, larger values of TCHP and BLT does not always mean that they are positively correlated to the TC intensity. In the present study, although the values of TCHP and BLT are higher over the SEAS region, it is unclear up to what depth the TC had interacted with the upper ocean and drawn its feedback. The earlier studies suggest that it is worth taking other elements like wind forcing, the speed of the storm, and upper ocean stratification into consideration as well. A recent study by Balaguru et al. (2015) suggested a new ocean metric, T_{dy} which accounts for all the above parameters and better represents the ocean feedback to the TC intensity changes. This metric has been tested in the Atlantic, Pacific and Southern Indian Ocean (Balaguru et al., 2015; Mawren & Reason, 2017) but not in the northern Indian Ocean. Hence, in the present study, we examined the depth up to which the impact of TC influenced the ocean by computing the value of mixing length at RI and RW locations.

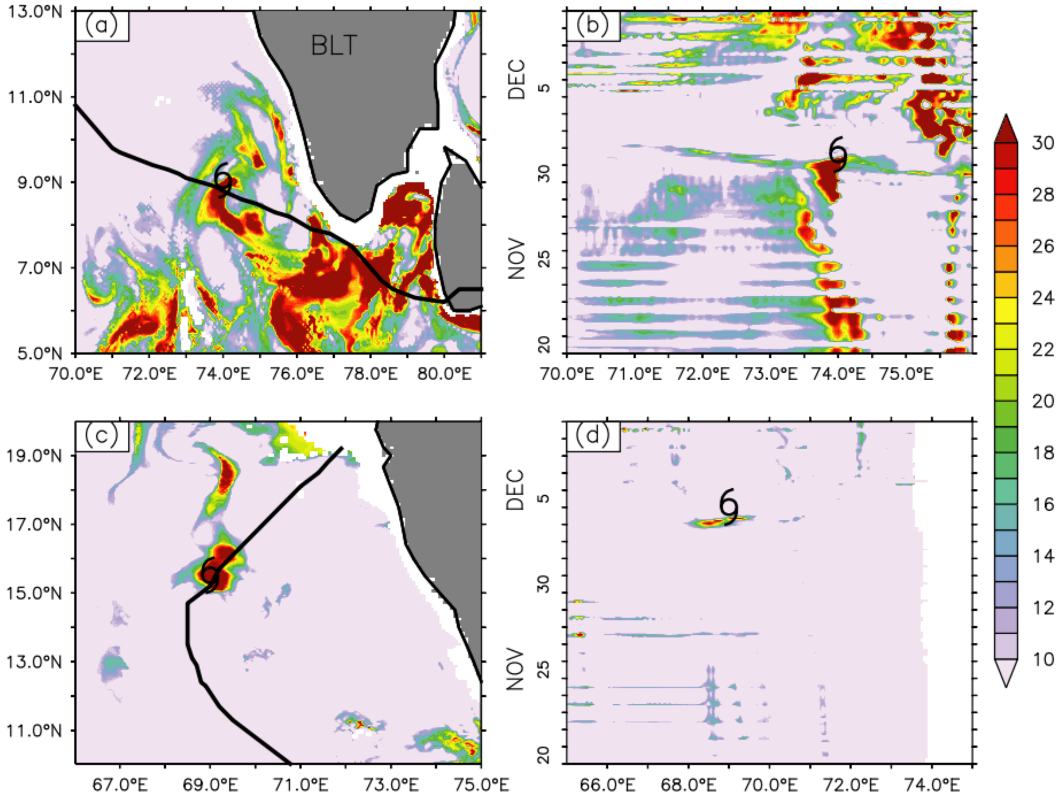

Figure 8. Same as Figure 7, but for BLT (m).

5.5 Evolution of temperature and salinity at RI and RW locations

There are marked differences in the evolution of upper-ocean thermohaline structure at RI and RW locations under the influence of TC Ockhi (Figure 9). The time-depth sections of temperature (a, c) and salinity (b, d) are examined from 28^{th} November to 14^{th} December from the surface to 150m depth. The cyclone symbol indicates the location of TC during the RI and RW stages. The overlaid contours represent the location of mixing length (black) and 26°C isotherm (cyan). Figure 9a shows the presence of warm waters ($> 28°$C) extending to deeper depths in the RI region compared to the RW region (Figure 9b), which is also evident from the position of 26°C isotherm overlaid (cyan contour). The arrival of TC reduced the surface temperatures by $\sim 2°$C at RW from 4^{th} December and continued to cool for the next few days, in contrast to the negligible cooling ($\sim 0.5°$C) in the RI region. While the thick warm layer at the RI location is barely disturbed with the passage of TC, there is a significant deepening of the mixed layer in case of RW, and the upper column of water continued to oscillate in the next few days. Apart from the thermal structure, the salinity (Figure 9b&d) at RI and RW show significant differences in vertical distribution. The RI location is capped with fresh waters before the arrival of TC. The source of these low saline waters had already been discussed in section 5.1 and explained using Figure 3. After the TC crossed this region, there is an increase in salinity by about 2PSU on 2^{nd} December. The RW location is occupied with high saline waters in the surface layer, and a marked shoaling of haloclines is evident in the subsurface layer, i.e., at around 100m depth on 4^{th} December. While comparing the RI and RW regions, the differences are more remarkable in the vertical structure of salinity than the temperature. We examined the salinity stratification in the surface layer before the TC arrival and its impact on TC intensity.

The vertical structure of salinity showed pronounced variations between the RI and RW locations, and thus significantly contributed to the density stratification along with the temperature as evident from Figure 9 . The mixing length is formulated by incorporating the information regarding the upper ocean stratification, TC speed, and the TC intensity. The near-surface ocean is highly stratified at RI while it is absent in the case of RW location. Besides ocean stability, the translation speed of TC Ockhi at the RI location is slower compared to the speed at RW (Figure 1b). Under lower translation speed, the storm churns the upper ocean for a longer time enhancing the vertical mixing. The TC intensity (in terms of maximum sustained wind speed) at the RI location is 50kn while the intensity at the RW location is 65kn. During the passage of TC Ockhi, the mixing length in Figure 9 (black contour) at RI location is 20m indicating the interaction of TC with the ocean is limited to this depth which is shallower than the depth of 26°C isotherm (80m) (cyan contour). As mentioned already, TCHP is simply the measure of ocean heat content up to 26°C isotherm, and hence, not necessarily indicate the mixing depth under the influence of TC. After the TC passage, there is a sharp recovery of the mixing length at the RI location and reached the pre-storm state quickly after one day. While the depth of the 26°C isotherm shoaled up to 50m on 2^{nd} December and came back to the normal state in a short time. On the other hand, at the RW location, the mixing length is extended up to 60m which is much deeper than the RI mixing length during the TC passage. This difference may be attributed to the lower stratification and more massive wind forcing that enhanced the mixing process at RW, which will be discussed in section 5.6. Interestingly, the depth of mixing length and 26°C isotherm are almost the same during the TC occurrence. However, the sharp rise of 26°C isotherm is more evident at RW location compared to RI. The surface waters at RW are cooled to < 26°C and it's depth has disappeared from 7^{th} December. Further, the differences between the depth of 26°C isotherm and mixing length are much larger in the case of RI than RW.

Thus, the above discussion reveals the potential problem of using TCHP alone as an intensity predictor in forecast models (DeMaria et al., 2005; Mainelli et al., 2008), especially RI storm cases. The fundamental reason is that the temperature under a storm is changing dynamically based on several factors, and these changes below the storm core are highly sensitive to the negative feedback to the TC.

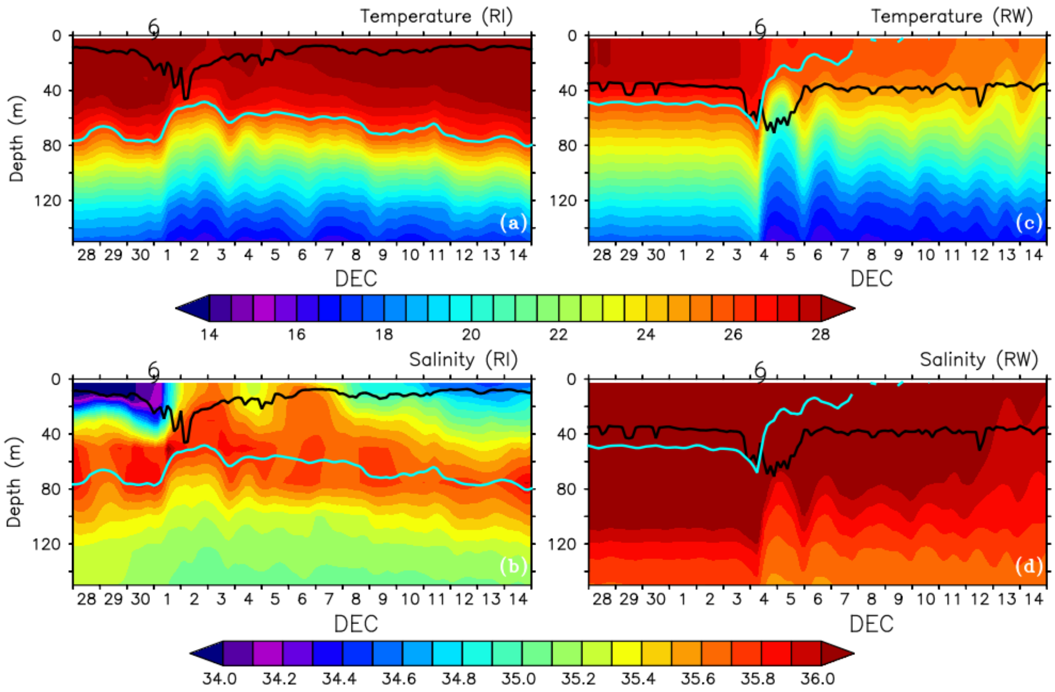

Figure 9. (a)Evolution of temperature at RI and (c) RW. (b) Salinity at RI and (d) RW locations. The black and cyan contours represent mixing length and depth of 26°C isotherm respectively.

Figure 10 presents the time series of upper ocean temperature averaged up to mixing length (T_{dy}) from RI and RW locations during 24^{th} November to 14^{th} December. The T_{dy} represents the dynamic temperature of the water column, which influenced the storm intensity. Dashed lines mark the time of the storm passage during RI and RW. The T_{dy} before the arrival of TC is ≈ 28.8°C, and dropped to below 28.5°C on 1^{st} December and further reduced to the minimum after one day on 2^{nd} December. The changes in T_{dy} at RI location were negligible before and after the TC Ockhi. On the other hand, T_{dy} was within the range of 27.5°C - 28°C at RW location before the storm and dropped to 24°C after the storm passage on 5^{th} December. The next day, the temperature was recovered to 26°C, and then the reduction continued for several days.

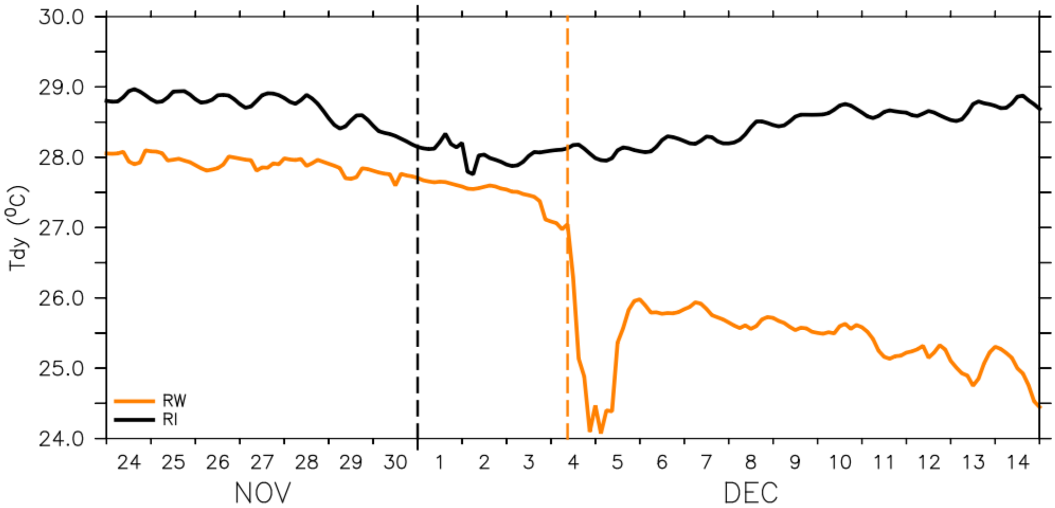

Figure 10. Time Series of the T_{dy} at RI and RW locations. The dashed vertical lines indicate the time of TC passage.

5.6 Ocean stratification during RI and RW stages

In this section, we further examine the contribution of stratification to the varying mixing lengths at RI and RW in terms of Richardson number (Ri) and it's components. The non-dimensional Ri is defined as the ratio of stratification to the shear squared.

$$Ri = \frac{N^2}{S^2} = \frac{-\frac{g}{\rho_o}\frac{\partial \rho}{\partial z}}{\frac{\partial u}{\partial z}^2 + \frac{\partial v}{\partial z}^2}$$

The square of the buoyancy frequency (N), Brunt Vaisala frequency (N^2) quantifies the importance of density stratification, where g is the acceleration due to gravity ($9.81\ ms^{-2}$), ρ_o is potential density and z is depth. The square of the velocity shear (S^2) is computed using eastward (u) and northward (v) components of velocity differences with respect to depth. Shear-induced instability occurs when Ri is less than 0.25 (Abarbanel et al., 1984; Howard, 1961; Miles, 1961). The reduced shear (S^2 - $4N^2$) is generally used as a proxy to differentiate the regions of turbulence from the stable layer. If S^2 - $4N^2$ is greater than zero, this implies that shear overcomes the stratification and leads to instability. Similarly, if S^2 - $4N^2$ is less than zero, then the instability is suppressed (Sanford et al., 2011).

To examine the variability in shear-induced turbulent mixing at RI and RW regions, N^2, S^2 and (S^2 - $4N^2$) are computed and shown in Figure 11. The left column and right column of Figure 11 represents the regions where RI (X=74°E, Y=8.8°N) and RW (X=69°E, Y=15.2°N) were initiated, respectively. The cyclone symbol indicates the storm location and the white contour in a) to d) marks the depth of the mixed layer. At the RI region in Figure 11a, the values of N^2 are higher in the pre-storm state (i.e., up to 30^{th} November) implying strong stratification at the surface. TC disturbed the stratification at the surface, and the N^2 values were reduced to nearly zero after its passage. Interestingly, the breakage of stratification is confined up to 30m in the surface layer despite the stronger TC wind forcing during this time. On the other hand, the surface layer at RW is not stratified as RI before the arrival of TC, which is evident from the values of N^2 (Figure 11b). The surface N^2 values were close to zero before and after the passage of TC in case of RW. However, there is an increase in stratification at the subsurface (~30

- 40m depth) after the passage of TC, i.e., on 5^{th} December. There is an increase in shear at the base of the mixed layer for both RI and RW stages as evident from Figure 11 c& d respectively. Stronger S^2 values are found between ∼30 - 60m depth in the RW region, while the values are weaker and shallower in case of RI (∼10 - 40m). The magnitude of shear at RW is strong enough to overcome the stratification and supported more mixing, unlike the RI region. Figure 11e&f represents the reduced shear for the RI and RW regions respectively and the thick brown line indicates the zero contour. The zero contour is much shallower (20m) in the RI region, compared to the RW region (50m). Thus, the shallow turbulence layer (20m) at RI and deeper one (50m) at RW are in agreement with the variability of mixing length.

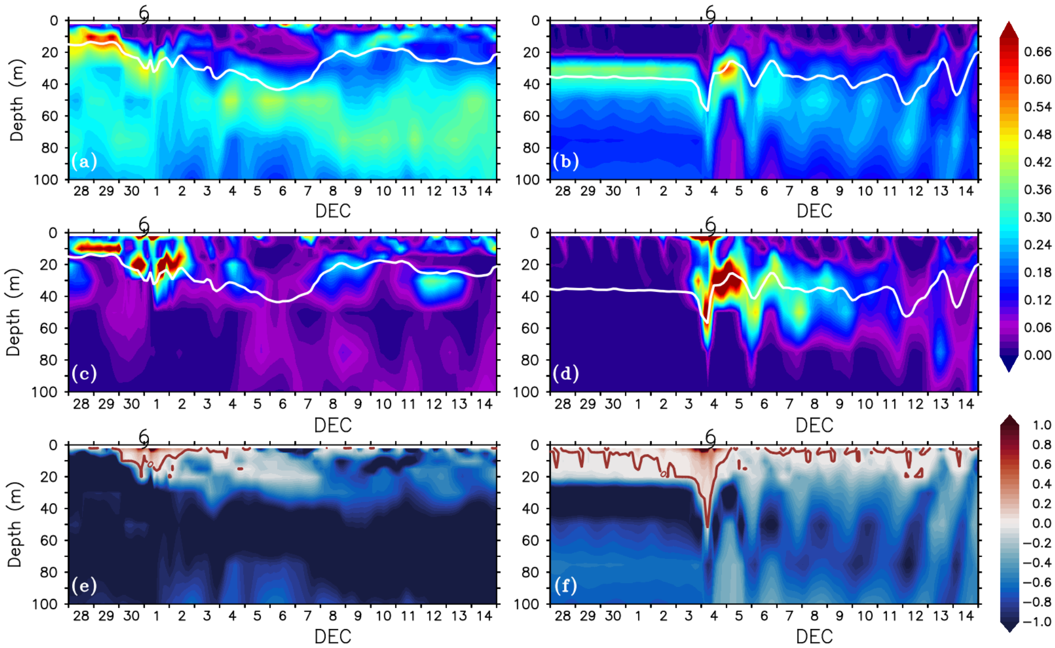

Figure 11. Time depth section of buoyancy frequency squared, shear squared, and reduced shear at RI (a, c, e) and RW (b, d, f) regions. The white contour from a)-d) indicates MLD. Brown contour in e) and f) represents the zero contour which demarcates the turbulent layer (positive values) from the stable layer (negative values).

6 Discussions and Conclusions

TC Ockhi was a rare storm in the AS in many aspects, including its unusual track, rapid development in the initial stages and rapid weakening before its landfall. In the present study, we explored the oceanic and atmospheric conditions prevailed before and during the RI and RW phases of TC Ockhi and related them to the storm intensity evolution. The analysis of the ocean profiles at RI and RW showed that the evolution of both thermal and haline structure under the influence of coastal current played a major role in the RI of TC Ockhi. Presence of thick warm layer (>26°C) of freshwater resulted in RI of the storm during 1^{st} December to 2^{nd} December. Distribution of mid-tropospheric humidity showed evidence for dry air intrusion over a weakly stratified ocean with a relatively thin warm layer of ocean leading to the RW phase of the storm. The impact of TC Ockhi on SST and subsurface at RI and RW were distinct. At RI location, the ocean was almost inert to the TC passage with just 0.8°C change in SST. The presence of thick (≈80 m) warm water(> 26°C) along with thick BL of a considerable spatial extent resisted the storm-induced cooling, though the storm was moving at a slow speed (2.5 m/s). This result is in contrary to several past studies which associated slow-moving storm to intense ocean cooling but in agreement with Lin et al. (2009), where she argued the presence of higher ocean heat content can reduce the ocean cooling and result in the intensification of the slow-moving storm.

Thus, in the case of TC Ockhi, the energy lost to the ocean at RI location was minimal, and the conditions favoured intensification as it passed slowly over a thick warm layer of the ocean. Strong currents close to the southern tip of India originated from BoB played a crucial role in propagating waters with thick BL and higher TCHP towards the RI location. There is strong evidence for BL formation associated with the transport of low saline waters from BoB under the influence of coastal currents. However, the mere presence of thick BL or high TCHP alone does not sustain the intensity of the storm. The combined influence of stratification, intensity and translation speed together with thermo-haline state of the ocean drove intensification and weakening of TC Ockhi. Previous studies showed that $\approx$ 60% of northern Indian Ocean storms out of 27 studied were not associated with high TCHP values. Though the presence of high TCHP at the RI stage of TC Ockhi explains the heat supply for storm intensification, in view of the contradicting reports, we have examined the new metric named T_{dy} which integrate temperature above variable mixing length and is a unique metric which takes into account of the role of translation speed, the intensity of the storm and thermo-haline stratification into account.

Comparison of mixing length with 26°C isotherm showed that the former is significantly shallower ($\approx$65m) than 26°C isotherm at RI location before and after the passage of the storm. However, the difference becomes negligible for a short duration during the passage of storm due to intense mixing. The analysis of the vertical section of salinity demonstrated the role of freshwater capping at RI location in bringing out the difference between 26°C isotherm and mixing length. We found that the stratification at RW location is mainly driven by temperature rather than salinity and is much weaker compared to the RI site. The difference between variable mixing length and 26°C isotherm is much lesser in the region of RW indicating lower stratification. After the passage of the storm, the 26°C isotherm outcropped, and thus estimation of TCHP became impractical. A relatively short-lived deepening of mixing length existed at RI compared to RW where it lasted for $\approx$2 days after the passage of storm . To summarize, given the diverse oceanic and atmospheric conditions crafting the destiny of a TC from its birth, it is not optimal to use a metric which factors in only temperature. A multi-parameter metric like T_{dy} will be more appropriate to get optimal results, particularly in salinity stratified regions. However, we require more case studies from the northern Indian Ocean for assuring the efficacy of the new metric, that can be taken up in the future.

Acknowledgments
We acknowledge the encouragement and infra-structural facilities provided by Dr. T. Srinivasa Kumar, Director, Indian National Centre for Ocean Information Services to carry out this work. We acknowledge the financial support from the Ministry of Earth Sciences (MoES) under the O-SMART program. The author(s) wish to acknowledge the use of the Ferret, NCL, and Python programs for analysis and graphics in this paper. Ferret is a product of NOAA's Pacific Marine Environmental Laboratory.

Data Availability Statement The atmospheric variables (wind, heat fluxes, RH) are available at the GFS website (`https://www.ncdc.noaa.gov/data-access/model-data/model-datasets/global-forcast-system-gfs`). The monthly averaged temperature and salinity profiles of EN4 data can be accessed at `http://www.metoffice.gov.uk/hadobs/en4/index.html`. TC related information can be accessed from IMD (`http://www.rsmcnewdelhi.imd.gov.in/index.php?option=com_content&view=article&id=48&Itemid=194&lang=en`) and IBTracs (`https://www.ncei.noaa.gov/data/international`

-best-track-archive-for-climate-stewardship-ibtracs/v04r00/access/netcdf/). All these data are made freely available. The HYCOM simulations of ocean parameters used in this manuscript can be requested from the institutional link http://www.incois.gov.in/portal/datainfo/insituhome.jsp.

References

Abarbanel, H. D., Holm, D. D., Marsden, J. E., & Ratiu, T. (1984). Richardson number criterion for the nonlinear stability of three-dimensional stratified flow. *Physical Review Letters*, *52*(26), 2352. doi: https://doi.org/10.1103/PhysRevLett.52.2352

Ali, M., Swain, D., Kashyap, T., McCreary, J., & Nagamani, P. (2012). Relationship between cyclone intensities and sea surface temperature in the tropical indian ocean. *IEEE Geoscience and Remote Sensing Letters*, *10*(4), 841–844. doi: https://doi.org/10.1109/LGRS.2012.2226138

Balaguru, K., Chang, P., Saravanan, R., Leung, L. R., Xu, Z., Li, M., & Hsieh, J.-S. (2012). Ocean barrier layers effect on tropical cyclone intensification. *Proceedings of the National Academy of Sciences*, *109*(36), 14343–14347. doi: https://doi.org/10.1073/pnas.1201364109

Balaguru, K., Foltz, G. R., Leung, L. R., Asaro, E. D., Emanuel, K. A., Liu, H., & Zedler, S. E. (2015). Dynamic potential intensity: An improved representation of the ocean's impact on tropical cyclones. *Geophysical Research Letters*, *42*(16), 6739–6746. doi: https://doi.org/10.1002/2015GL064822

Bender, M. A., Ginis, I., & Kurihara, Y. (1993). Numerical simulations of tropical cyclone-ocean interaction with a high-resolution coupled model. *Journal of Geophysical Research: Atmospheres*, *98*(D12), 23245–23263. doi: https://doi.org/10.1029/93JD02370

Bhatia, K. T., Vecchi, G. A., Knutson, T. R., Murakami, H., Kossin, J., Dixon, K. W., & Whitlock, C. E. (2019). Recent increases in tropical cyclone intensification rates. *Nature communications*, *10*(1), 1–9. doi: https://doi.org/10.1038/s41467-019-08471-z

Bosart, L. F., Bracken, W. E., Molinari, J., Velden, C. S., & Black, P. G. (2000). Environmental influences on the rapid intensification of hurricane opal (1995) over the gulf of mexico. *Monthly Weather Review*, *128*(2), 322–352. doi: https://doi.org/10.1175/1520-0493(2000)128⟨0322:EIOTRI⟩2.0.CO;2

Brand, S. (1971). The effects on a tropical cyclone of cooler surface waters due to upwelling and mixing produced by a prior tropical cyclone. *Journal of Applied Meteorology*, *10*(5), 865–874. doi: https://doi.org/10.1175/1520-0450(1971)010⟨0865:TEOATC⟩2.0.CO;2

Byers, H. R. (1959). *General meteorology.* doi: https://doi.org/10.1002/qj.49708636716

Chang, Y.-T., Lin, I., Huang, H.-C., Liao, Y.-C., & Lien, C.-C. (2020). The association of typhoon intensity increase with translation speed increase in the south china sea. *Sustainability*, *12*(3), 939. doi: https://doi.org/10.3390/su12030939

Chaudhuri, D., Sengupta, D., DAsaro, E., Venkatesan, R., & Ravichandran, M. (2019). Response of the salinity-stratified bay of bengal to cyclone phailin. *Journal of Physical Oceanography*, *49*(5), 1121–1140. doi: https://doi.org/10.1175/JPO-D-18-0051.1

Cione, J. J., & Uhlhorn, E. W. (2003). Sea surface temperature variability in hurricanes: Implications with respect to intensity change. *Monthly Weather Review*, *131*(8), 1783–1796. doi: https://10.1175//2562.1

Dare, R. A., & McBride, J. L. (2011). Sea surface temperature response to tropical cyclones. *Monthly Weather Review*, *139*(12), 3798–3808. doi: https://doi.org/10.1175/MWR-D-10-05019.1

DeMaria, M. (1996). The effect of vertical shear on tropical cyclone intensity change. *Journal of the atmospheric sciences*, *53*(14), 2076–2088. doi: https://doi.org/10.1175/1520-0469(1996)053⟨2076:TEOVSO⟩2.0.CO;2

DeMaria, M., Mainelli, M., Shay, L. K., Knaff, J. A., & Kaplan, J. (2005). Further improvements to the statistical hurricane intensity prediction scheme (ships). *Weather and Forecasting*, *20*(4), 531–543. doi: https://doi.org/10.1175/WAF862.1

Donelan, M., Haus, B. K., Reul, N., Plant, W., Stiassnie, M., Graber, H. C., . . . Saltzman, E. (2004). On the limiting aerodynamic roughness of the ocean in very strong winds. *Geophysical Research Letters*, *31*(18). doi: https://doi.org/10.1029/2004GL019460

Elsberry, R. L. (2014). Advances in research and forecasting of tropical cyclones from 1963–2013. *Asia-Pacific Journal of Atmospheric Sciences*, *50*(1), 3–16. doi: https://doi.org/10.1007/s13143-014-0001-1

Emanuel, K. (2003). Tropical cyclones. *Annual review of earth and planetary sciences*, *31*(1), 75-104. doi: https://10.1146/annurev.earth.31.100901.141259

Emanuel, K. (2017). Will global warming make hurricane forecasting more difficult? *Bulletin of the American Meteorological Society*, *98*(3), 495–501. doi: https://doi.org/10.1175/BAMS-D-16-0134.1

Emanuel, K. A. (1986). An air-sea interaction theory for tropical cyclones. part i: Steady-state maintenance. *Journal of the Atmospheric Sciences*, *43*(6), 585–605. doi: https://doi.org/10.1175/1520-0469(1986)043⟨0585:AASITF⟩2.0.CO;2

Evan, A. T., & Camargo, S. J. (2011). A climatology of arabian sea cyclonic storms. *Journal of Climate*, *24*(1), 140–158. doi: https://doi.org/10.1175/2010JCLI3611.1

Evans, J. L. (1993). Sensitivity of tropical cyclone intensity to sea surface temperature. *Journal of Climate*, *6*(6), 1133–1140. doi: https://doi.org/10.1175/1520-0442(1993)006⟨1133:SOTCIT⟩2.0.CO;2

Foltz, G. R., & McPhaden, M. J. (2009). Impact of barrier layer thickness on sst in the central tropical north atlantic. *Journal of Climate*, *22*(2), 285–299. doi: https://doi.org/10.1175/2008JCLI2308.1

Frank, N. L., & Husain, S. (1971). The deadliest tropical cyclone in history? *Bulletin of the American Meteorological Society*, *52*(6), 438–445. doi: https://doi.org/10.1175/1520-0477(1971)052⟨0438:TDTCIH⟩2.0.CO;2

Ganguly, D., Suryanarayana, K., & Raman, M. (2020). Cyclone ockhi induced upwelling and associated changes in biological productivity in arabian sea. *Marine Geodesy*, 1–14. doi: https://doi.org/10.1080/01490419.2020.1838675

Gao, S., Zhang, W., Liu, J., Lin, I.-I., Chiu, L. S., & Cao, K. (2016). Improvements in typhoon intensity change classification by incorporating an ocean coupling potential intensity index into decision trees. *Weather and Forecasting*, *31*(1), 95–106. doi: https://doi.org/10.1175/WAF-D-15-0062.1

Goni, J., G., Knaff, J., & Lin, I. (2007). Tropical cyclone heat potential. *State of the Climate in*, 43–45.

Goni, J., G., & Trinanes, J. A. (2003). Ocean thermal structure monitoring could aid in the intensity forecast of tropical cyclones. *Eos, Transactions American Geophysical Union*, *84*(51), 573–578. doi: https://doi.org/10.1029/2003EO510001

Gray, W. M. (1968). Global view of the origin of tropical disturbances and storms. *Monthly Weather Review*, *96*(10), 669–700. doi: https://doi.org/10.1175/1520-0493(1968)096⟨0669:GVOTOO⟩2.0.CO;2

Guinn, T. A., & Schubert, W. H. (1993). Hurricane spiral bands. *Journal of the atmospheric sciences*, *50*(20), 3380–3403. doi: https://doi.org/10.1175/1520-0469(1993)050⟨3380:HSB⟩2.0.CO;2

Hill, K. A., & Lackmann, G. M. (2009). Influence of environmental humidity on tropical cyclone size. *Monthly Weather Review*, *137*(10), 3294–3315. doi: https://doi.org/10.1175/2009MWR2679.1

Holliday, C. R., & Thompson, A. H. (1979). Climatological characteristics of rapidly intensifying typhoons. *Monthly Weather Review*, *107*(8), 1022–1034. doi: https://doi.org/10.1175/JCLI-D-17-0653.1

Howard, L. N. (1961). Note on a paper of john w. miles. *Journal of Fluid Mechanics*, *10*(4), 509–512. doi: https://doi.org/10.1017/S0022112061000317

Jacob, S. D., Shay, L. K., Mariano, A. J., & Black, P. G. (2000). The 3d oceanic mixed layer response to hurricane gilbert. *Journal of Physical Oceanography*, *30*(6), 1407–1429. doi: https://doi.org/10.1175/1520-0485(2000)030⟨1407:TOMLRT⟩2.0.CO;2

Jaimes, B., Shay, L. K., & Uhlhorn, E. W. (2015). Enthalpy and momentum fluxes during hurricane earl relative to underlying ocean features. *Monthly Weather Review*, *143*(1), 111–131. doi: https://doi.org/10.1175/MWR-D-13-00277.1

Jangir, B., Swain, D., & Bhaskar, T. U. (2016). Relation between tropical cyclone heat potential and cyclone intensity in the north indian ocean. In *Remote sensing and modeling of the atmosphere, oceans, and interactions vi* (Vol. 9882, p. 988228). doi: https://doi.org/10.1117/12.2228033

Kaplan, J., & DeMaria, M. (2003). Large-scale characteristics of rapidly intensifying tropical cyclones in the north atlantic basin. *Weather and forecasting*, *18*(6), 1093–1108. doi: https://doi.org/10.1175/1520-0434(2003)018⟨1093:LCORIT⟩2.0.CO;2

Kaplan, J., DeMaria, M., & Knaff, J. A. (2010). A revised tropical cyclone rapid intensification index for the atlantic and eastern north pacific basins. *Weather and forecasting*, *25*(1), 220–241. doi: https://doi.org/10.1175/2009WAF2222280.1

Kara, A. B., Rochford, P. A., & Hurlburt, H. E. (2003). Mixed layer depth variability over the global ocean. *Journal of Geophysical Research: Oceans*, *108*(C3). doi: https://doi.org/10.1029/2000JC000736

Kashem, M., Ahmed, M. K., Qiao, F., Akhter, M., & Chowdhury, K. A. (2019). The response of the upper ocean to tropical cyclone viyaru over the bay of bengal. *Acta Oceanologica Sinica*, *38*(1), 61–70. doi: https://doi.org/10.1007/s13131-019-1370-1

Kimball, S. K. (2006). A modeling study of hurricane landfall in a dry environment. *Monthly weather review*, *134*(7), 1901–1918. doi: https://doi.org/10.1175/MWR3155.1

Komaromi, W. A. (2013). An investigation of composite dropsonde profiles for developing and nondeveloping tropical waves during the 2010 predict field campaign. *Journal of the atmospheric sciences*, *70*(2), 542–558. doi: https://doi.org/10.1175/JAS-D-12-052.1

Kotal, S., Bhattacharya, S., Bhowmik, S. R., & Kundu, P. (2014). Growth of cyclone viyaru and phailin–a comparative study. *Journal of Earth System Science*, *123*(7), 1619–1635. doi: https://doi.org/10.1007/s12040-014-0493-1

Kotal, S., & Roy Bhowmik, S. (2013). Large-scale characteristics of rapidly intensifying tropical cyclones over the bay of bengal and a rapid intensification (ri) index. *Mausam*, *64*(1), 13–24. doi: https://doi.org/10.1175/1520-0434(2003)018⟨1093:LCORIT⟩2.0.CO;2

Krishnamurti, T., Pattnaik, S., Stefanova, L., Kumar, T. V., Mackey, B. P., Oshay, A., & Pasch, R. J. (2005). The hurricane intensity issue. *Monthly weather review*, *133*(7), 1886–1912. doi: https://doi.org/10.1175/MWR2954.1

Kumar, P., & Mathew, B. (1997). Salinity distribution in the arabian sea. *Indian Journal of Marine Sciences*, *26*, 271-277.

Leipper, D. F., & Volgenau, D. (1972). Hurricane heat potential of the gulf of mexico. *Journal of Physical Oceanography*, *2*(3), 218–224. doi: http://dx.doi.org/10.1175/1520-0485(1972)002⟨0218:HHPOTG⟩2.0.CO;2

Le Marshall, J., Leslie, L., Abbey Jr, R., & Qi, L. (2002). Tropical cyclone track and intensity prediction: The generation and assimilation of high-density, satellite-derived data. *Meteorology and Atmospheric Physics*, *80*(1-4), 43–57. doi: https://doi.org/10.1007/s007030200013

Lin, I. I., Goni, G. J., Knaff, J. A., Forbes, C., & Ali, M. M. (2012). Ocean heat content for tropical cyclone intensity forecasting and its impact on storm surge. *Natural Hazards*, *66*(3), 1481-1500. doi: https://doi.org/10.1007/s11069-012-0214-5

Lin, I. I., Pun, I.-F., & Wu, C.-C. (2009, 11). Upper-ocean thermal structure and the western north pacific category 5 typhoons. part ii: Dependence on translation speed. *Monthly Weather Review*, *137*(11), 3744–3757. doi: https://doi.org/10.1175/2009MWR2713.1

Lin, I. I., Wu, C.-C., Pun, I.-F., & Ko, D.-S. (2008). Upper-ocean thermal structure and the western north pacific category 5 typhoons. part i: Ocean features and the category 5 typhoons intensification. *Monthly Weather Review*, *136*(9), 3288–3306. doi: https://doi.org/10.1175/2008MWR2277.1

Lloyd, I. D., & Vecchi, G. A. (2011). Observational evidence for oceanic controls on hurricane intensity. *Journal of Climate*, *24*(4), 1138–1153. doi: https://doi.org/10.1175/2010JCLI3763.1

Lü, H., Zhao, X., Sun, J., Zha, G., Xi, J., & Cai, S. (2020). A case study of a phytoplankton bloom triggered by a tropical cyclone and cyclonic eddies. *PloS one*, *15*(4), e0230394. doi: https://doi.org/10.1371/journal.pone.0230394

Luis, A. J., & Kawamura, H. (2003). Seasonal sst patterns along the west india shelf inferred from avhrr. *Remote sensing of environment*, *86*(2), 206–215. doi: https://doi.org/10.1016/S0034-4257(03)00101-9

Mainelli, M., DeMaria, M., Shay, L. K., & Goni, G. (2008). Application of oceanic heat content estimation to operational forecasting of recent atlantic category 5 hurricanes. *Weather and Forecasting*, *23*(1), 3–16. doi: https://doi.org/10.1175/2007WAF2006111.1

Malkus, J. S., & Riehl, H. (1960). On the dynamics and energy transformations in steady-state hurricanes. *Tellus*, *12*(1), 1–20. doi: https://doi.org/10.1111/j.2153-3490.1960.tb01279.x

Marks, F. D., Shay, L. K., & PDT-5. (1998). Landfalling tropical cyclones: Forecast problems and associated research opportunities. *Bulletin of the American Meteorological Society*, *79*(2), 305–323. doi: https://10.1175/1520-0477(1998)079⟨0305:LTCFPA⟩2.0.CO;2

Mawren, D., & Reason, C. (2017). Variability of upper-ocean characteristics and tropical cyclones in the south west indian ocean. *Journal of Geophysical Research: Oceans*, *122*(3), 2012–2028. doi: https://doi.org/10.1002/2016JC012028

Mei, W., Pasquero, C., & Primeau, F. (2012). The effect of translation speed upon the intensity of tropical cyclones over the tropical ocean. *Geophysical Research Letters*, *39*(7). doi: https://doi.org/10.1029/2011GL050765

Miles, J. W. (1961). On the stability of heterogeneous shear flows. *Journal of Fluid Mechanics*, *10*(4), 496–508. doi: https://doi.org/10.1017/S0022112061000305

Miller, B. I. (1958). On the maximum intensity of hurricanes. *Journal of Meteorology*, *15*(2), 184–195. doi: https://doi.org/10.1175/1520-0469(1958)015⟨0184:OTMIOH⟩2.0.CO;2

Mohanty, U., Nadimpalli, R., Mohanty, S., & Osuri, K. K. (2019). Recent advancements in prediction of tropical cyclone track over north indian ocean basin. *MAUSAM*, *70*(1), 57–70.

Mohanty, U. C., & Gopalakrishnan, S. G. (2016). *Advanced numerical modeling and data assimilation techniques for tropical cyclone predictions*. Springer.

Molinari, J., & Vollaro, D. (2010). Rapid intensification of a sheared tropical storm. *Monthly weather review*, *138*(10), 3869–3885. doi: https://doi.org/10.1175/

2010MWR3378.1
Monaldo, F. M., Sikora, T. D., Babin, S. M., & Sterner, R. E. (1997). Satellite imagery of sea surface temperature cooling in the wake of hurricane edouard (1996). *Monthly Weather Review*, *125*(10), 2716–2721. doi: 10.1175/1520-0493(1997)125⟨2716:SIOSST⟩2.0.CO;2
Montgomery, M. T., Persing, J., & Smith, R. K. (2015). Putting to rest wisheful misconceptions for tropical cyclone intensification. *Journal of Advances in Modeling Earth Systems*, *7*(1), 92–109. doi: https://doi.org/10.1002/2014MS000362
Neetu, S., Lengaigne, M., Vincent, E. M., Vialard, J., Madec, G., Samson, G., ... Durand, F. (2012). Influence of upper-ocean stratification on tropical cyclone-induced surface cooling in the bay of bengal. *Journal of Geophysical Research: Oceans*, *117*(C12). doi: https://doi.org/10.1029/2012JC008433
Nolan, D. (2006). What is the trigger for tropical cyclogenesis. *Australian Meteorological Magazine*, *56*, 241-266.
Nyadjro, E. S., Subrahmanyam, B., Murty, V., & Shriver, J. F. (2012). The role of salinity on the dynamics of the arabian sea mini warm pool. *Journal of Geophysical Research: Oceans*, *117*(C9). doi: https://doi.org/10.1029/2012JC007978
Ooyama, K. (1969). Numerical simulation of the life cycle of tropical cyclones. *Journal of the Atmospheric Sciences*, *26*(1), 3–40. doi: https://doi.org/10.1175/1520-0469(1969)026⟨0003:NSOTLC⟩2.0.CO;2
Park, M.-S., Elsberry, R. L., & Harr, P. A. (2012). Vertical wind shear and ocean heat content as environmental modulators of western north pacific tropical cyclone intensification and decay. *Tropical Cyclone Research and Review*, *1*(4), 448–457. doi: https://doi.org/10.6057/2012TCRR04.03
Price, J. F. (1981). Upper ocean response to a hurricane. *Journal of Physical Oceanography*, *11*(2), 153–175. doi: https://doi.org/10.1175/1520-0485(1981)011⟨0153:UORTAH⟩2.0.CO;2
Price, J. F., Morzel, J., & Niiler, P. P. (2008). Warming of sst in the cool wake of a moving hurricane. *Journal of Geophysical Research: Oceans*, *113*(C7). doi: https://doi.org/10.1029/2007JC004393
Riehl, H., & Shafer, R. J. (1944). The recurvature of tropical storms. *Journal of Meteorology*, *1*(1), 42–54. doi: https://doi.org/10.1175/1520-0469(1944)001⟨0001:TROTS⟩2.0.CO;2
Rotunno, R., & Emanuel, K. A. (1987). An air–sea interaction theory for tropical cyclones. part ii: Evolutionary study using a nonhydrostatic axisymmetric numerical model. *Journal of the Atmospheric Sciences*, *44*(3), 542–561. doi: https://doi.org/10.1175/1520-0469(1987)044⟨0542:AAITFT⟩2.0.CO;2
Sanap, S., Mohapatra, M., Ali, M., Priya, P., & Varaprasad, D. (2020). On the dynamics of cyclogenesis, rapid intensification and recurvature of the very severe cyclonic storm, ockhi. *Journal of Earth System Science*, *129*(1), 1–13. doi: https://doi.org/10.1007/s12040-020-01457-2
Sanford, T. B., Price, J. F., & Girton, J. B. (2011). Upper-ocean response to hurricane frances (2004) observed by profiling em-apex floats. *Journal of Physical Oceanography*, *41*(6), 1041–1056. doi: https://doi.org/10.1175/2010JPO4313.1
Schade, L. R., & Emanuel, K. A. (1999). The oceans effect on the intensity of tropical cyclones: Results from a simple coupled atmosphere–ocean model. *Journal of the Atmospheric Sciences*, *56*(4), 642–651. doi: https://doi.org/10.1175/1520-0469(1999)056⟨0642:TOSEOT⟩2.0.CO;2
Sengupta, D., Goddalehundi, B. R., & Anitha, D. (2008). Cyclone-induced mixing does not cool sst in the post-monsoon north bay of bengal. *Atmospheric Science Letters*, *9*(1), 1–6. doi: https://doi.org/10.1002/asl.162
Shay, L. K., Black, P. G., Mariano, A. J., Hawkins, J. D., & Elsberry, R. L. (1992).

Upper ocean response to hurricane gilbert. *Journal of Geophysical Research: Oceans*, *97*(C12), 20227–20248. doi: https://doi.org/10.1029/92JC01586

Shay, L. K., & Brewster, J. K. (2010). Oceanic heat content variability in the eastern pacific ocean for hurricane intensity forecasting. *Monthly Weather Review*, *138*(6), 2110–2131. doi: https://doi.org/10.1175/2010MWR3189.1

Shay, L. K., Goni, G. J., & Black, P. G. (2000). Effects of a warm oceanic feature on hurricane opal. *Monthly Weather Review*, *128*(5), 1366–1383. doi: 10.1175/1520-0493(2000)128⟨1366:EOAWOF⟩2.0.CO;2

Shenoi, S., Shankar, D., Gopalakrishna, V., & Durand, F. (2005). Role of ocean in the genesis and annihilation of the core of the warm pool in the southeastern arabian sea. *Mausam*, *56*(1), 147–160.

Simpson, R., Bureau, U. W., & Riehl, H. (1958). Mid-tropospheric ventilation as a constraint on hurricane development and maintenance. In *Presented at proceedings of the ams technical conference on hurricanes.* doi: 10.1145/2601097.2601185

Singh, V. K., Roxy, M., & Deshpande, M. (2020). The unusual long track and rapid intensification of very severe cyclone ockhi. *CURRENT SCIENCE*, *119*(5), 771–779. doi: 10.18520/cs/v119/i5/771-779

Smith, R. K., & Montgomery, M. T. (2012). Observations of the convective environment in developing and non-developing tropical disturbances. *Quarterly Journal of the Royal Meteorological Society*, *138*(668), 1721–1739. doi: https://doi.org/10.1002/qj.1910

Sprintall, J., & Tomczak, M. (1992). Evidence of the barrier layer in the surface layer of the tropics. *Journal of Geophysical Research: Oceans*, *97*(C5), 7305–7316. doi: https://doi.org/10.1029/92JC00407

Srinivas, K., & Kumar, P. D. (2006). Atmospheric forcing on the seasonal variability of sea level at cochin, southwest coast of india. *Continental shelf research*, *26*(10), 1113–1133. doi: https://doi.org/10.1016/j.csr.2006.03.010

Stramma, L., Cornillon, P., & Price, J. F. (1986). Satellite observations of sea surface cooling by hurricanes. *Journal of Geophysical Research: Oceans*, *91*(C4), 5031–5035. doi: 10.1029/JC091iC04p05031

Sun, Y., Zhong, Z., Li, T., Yi, L., Hu, Y., Wan, H., … Li, Q. (2017). Impact of ocean warming on tropical cyclone size and its destructiveness. *Scientific reports*, *7*(1), 1–10. doi: https://doi.org/10.1038/s41598-017-08533-6

Tang, B., & Emanuel, K. (2010). Midlevel ventilations constraint on tropical cyclone intensity. *Journal of the Atmospheric Sciences*, *67*(6), 1817–1830. doi: https://doi.org/10.1175/2010JAS3318.1

Vincent, E. M., Lengaigne, M., Madec, G., Vialard, J., Samson, G., Jourdain, N. C., … Jullien, S. (2012). Processes setting the characteristics of sea surface cooling induced by tropical cyclones. *Journal of Geophysical Research: Oceans*, *117*(C2). doi: https://doi.org/10.1029/2011JC007396

Wang, X., Han, G., Qi, Y., & Li, W. (2011). Impact of barrier layer on typhoon-induced sea surface cooling. *Dynamics of Atmospheres and Oceans*, *52*(3), 367–385. doi: https://doi.org/10.1029/2007JC004393

Wang, Y., & Wu, C.-C. (2004). Current understanding of tropical cyclone structure and intensity changes–a review. *Meteorology and Atmospheric Physics*, *87*(4), 257–278. doi: https://doi.org/10.1007/s00703-003-0055-6

Willoughby, H., Clos, J., & Shoreibah, M. (1982). Concentric eye walls, secondary wind maxima, and the evolution of the hurricane vortex. *Journal of the Atmospheric Sciences*, *39*(2), 395–411. doi: https://doi.org/10.1175/1520-0469(1982)039⟨0395:CEWSWM⟩2.0.CO;2

Wong, M. L., & Chan, J. C. (2004). Tropical cyclone intensity in vertical wind shear. *Journal of the atmospheric sciences*, *61*(15), 1859–1876. doi: https://doi.org/10.1175/1520-0469(2004)061⟨1859:TCIIVW⟩2.0.CO;2

Wood, K. M., & Ritchie, E. A. (2015). A definition for rapid weakening of north atlantic and eastern north pacific tropical cyclones. *Geophysical Research Letters*, *42*(22), 10–091. doi: https://doi.org/10.1002/2015GL066697

Wu, L., Su, H., Fovell, R., Dunkerton, T., Wang, Z., & Kahn, B. (2015). Impact of environmental moisture on tropical cyclone intensification. *Atmospheric Chemistry and Physics*, *15*(24), 14041–14053. doi: https://doi.org/10.5194/acp-15-14041-2015

Yan, Y., Li, L., & Wang, C. (2017). The effects of oceanic barrier layer on the upper ocean response to tropical cyclones. *Journal of Geophysical Research: Oceans*, *122*(6), 4829–4844. doi: https://doi.org/10.1002/2017JC012694

Zedler, S. E. (2009). Simulations of the ocean response to a hurricane: Nonlinear processes. *Journal of physical oceanography*, *39*(10), 2618–2634. doi: https://doi.org/10.1175/2009JPO4062.1

Figure1.pdf.

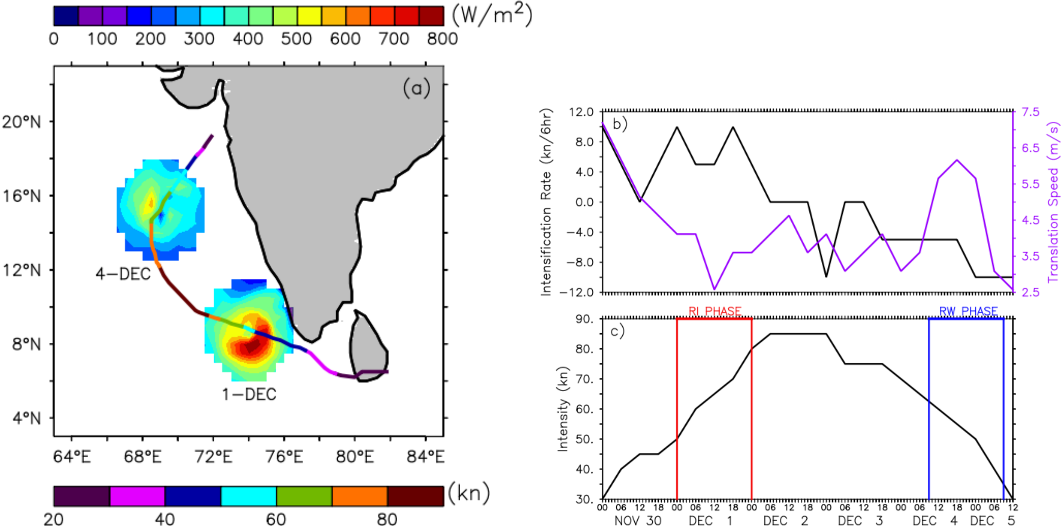
(W/m2)
0 100 200 300 400 500 600 700 800
(a)
20°N
16°N
12°N
8°N
4°N
64°E 68°E 72°E 76°E 80°E 84°E
4—DEC
1—DEC
(kn)
20 40 60 80
b)
Intensification Rate (kn/6hr)
Translation Speed (m/s)
12.0 8.0 4.0 0.0 −4.0 −8.0 −12.0
7.5 6.5 5.5 4.5 3.5 2.5
RI PHASE
RW PHASE
c)
Intensity (kn)
90. 80. 70. 60. 50. 40. 30.
00 06 12 18 00 06 12 18 00 06 12 18 00 06 12 18 00 06 12 18 00 06 12
NOV 30 DEC 1 DEC 2 DEC 3 DEC 4 DEC 5

Figure2.pdf.

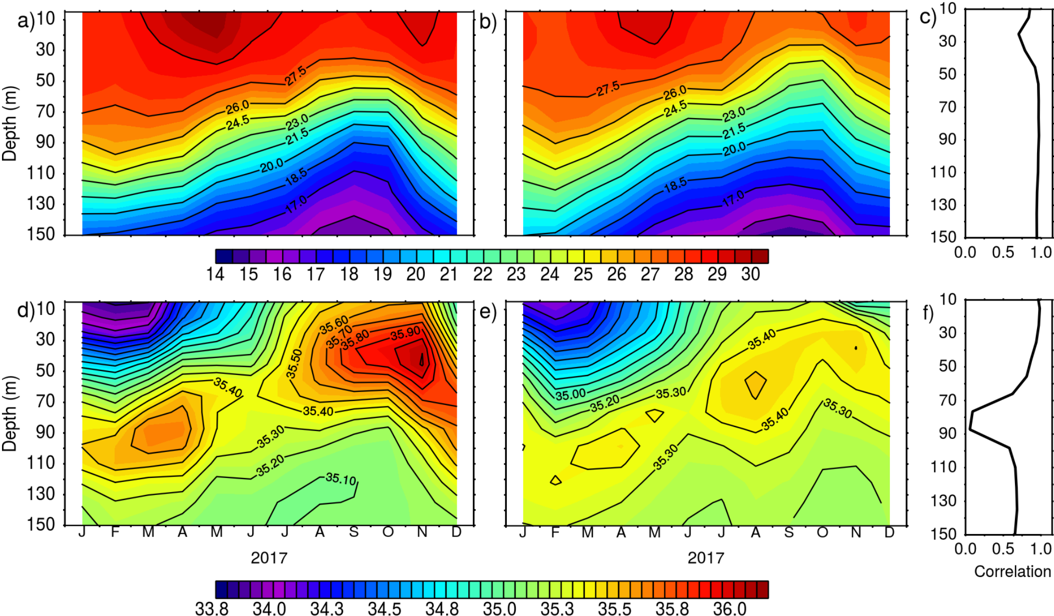
a)
b)
c)
d)
e)
f)
Depth (m)
10
30
50
70
90
110
130
150
27.5
26.0
24.5
23.0
21.5
20.0
18.5
17.0
0.0
0.5
1.0
14
15
16
17
18
19
20
21
22
23
24
25
26
27
28
29
30
35.60
35.70
35.80
35.90
35.50
35.40
35.30
35.20
35.10
35.00
J
F
M
A
M
J
J
A
S
O
N
D
2017
Correlation
33.8
34.0
34.3
34.5
34.8
35.0
35.3
35.5
35.8
36.0

Figure3.pdf.

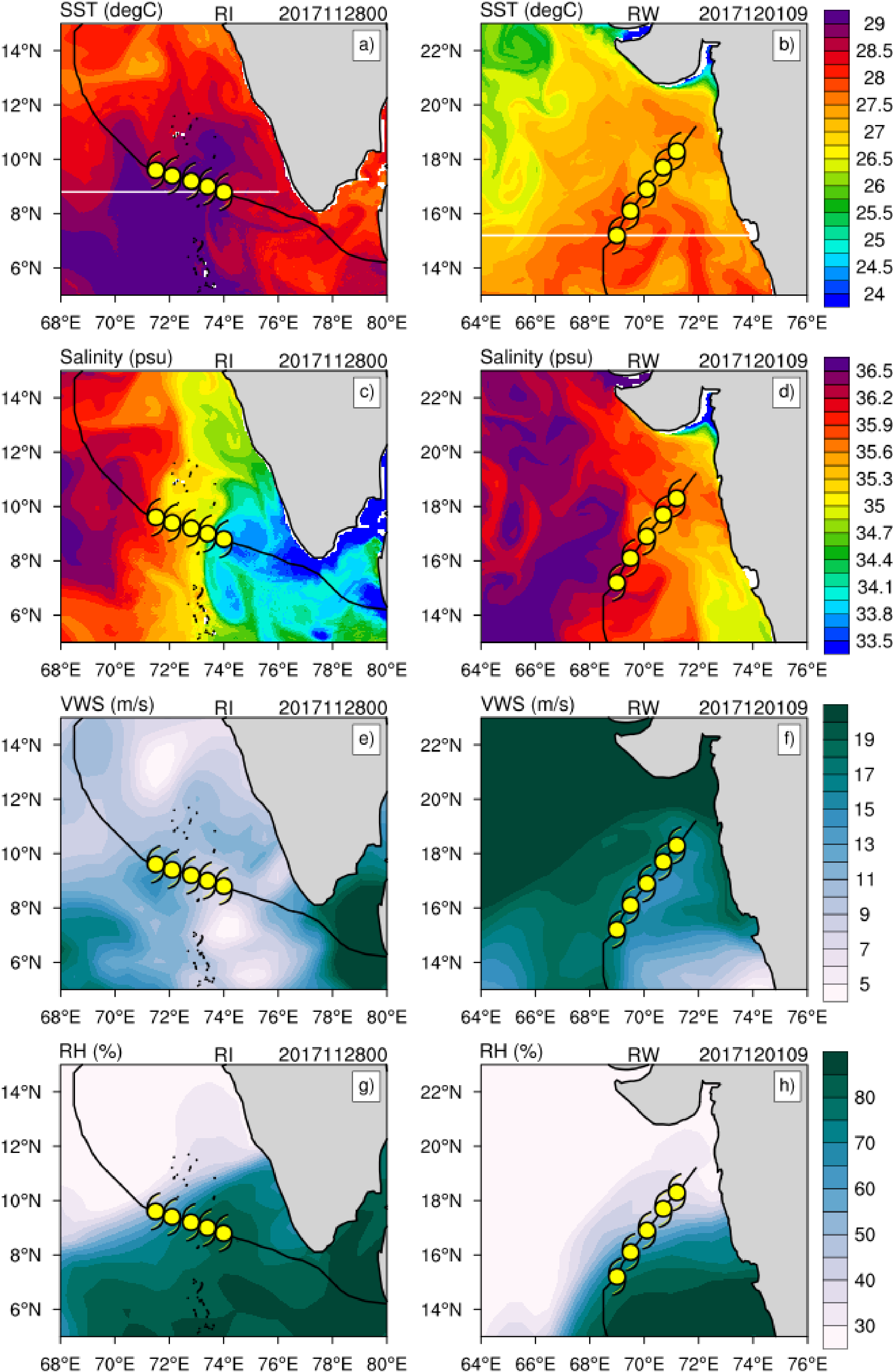

SST (degC) RI 2017112800
a)
SST (degC) RW 2017120109
b)
29
28.5
28
27.5
27
26.5
26
25.5
25
24.5
24
Salinity (psu) RI 2017112800
c)
Salinity (psu) RW 2017120109
d)
36.5
36.2
35.9
35.6
35.3
35
34.7
34.4
34.1
33.8
33.5
VWS (m/s) RI 2017112800
e)
VWS (m/s) RW 2017120109
f)
19
17
15
13
11
9
7
5
RH (%) RI 2017112800
g)
RH (%) RW 2017120109
h)
80
70
60
50
40
30
14°N
12°N
10°N
8°N
6°N
22°N
20°N
18°N
16°N
14°N
68°E 70°E 72°E 74°E 76°E 78°E 80°E
64°E 66°E 68°E 70°E 72°E 74°E 76°E

Figure4.pdf.

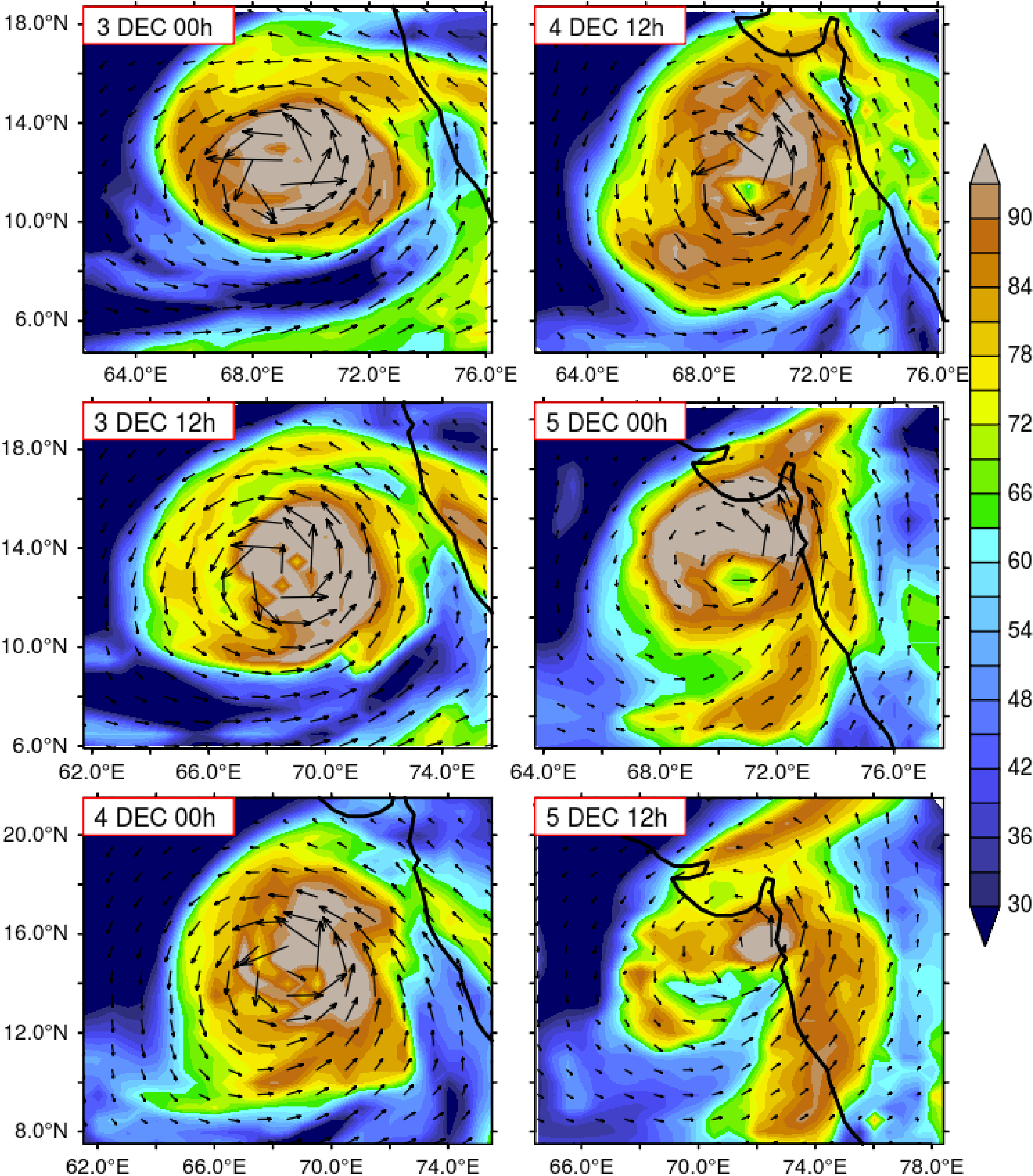
3 DEC 00h
4 DEC 12h
3 DEC 12h
5 DEC 00h
4 DEC 00h
5 DEC 12h
18.0°N
14.0°N
10.0°N
6.0°N
20.0°N
16.0°N
12.0°N
8.0°N
62.0°E
64.0°E
66.0°E
68.0°E
70.0°E
72.0°E
74.0°E
76.0°E
78.0°E
90
84
78
72
66
60
54
48
42
36
30

Figure5.pdf.

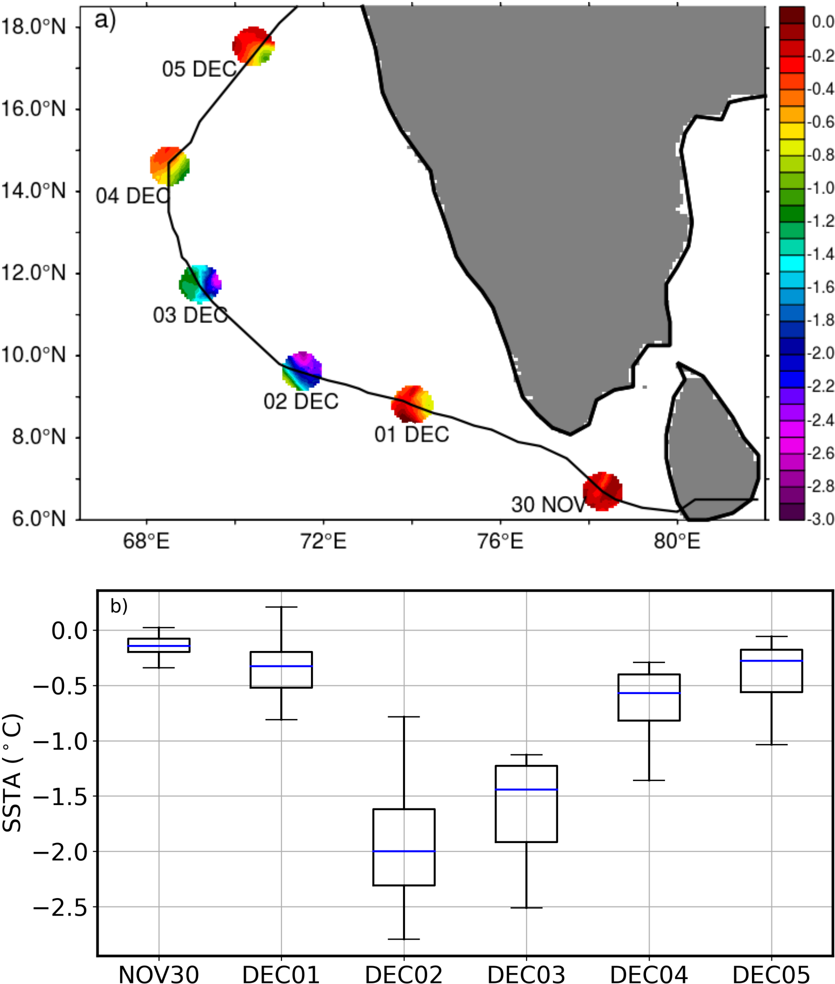
a)
18.0°N
16.0°N
14.0°N
12.0°N
10.0°N
8.0°N
6.0°N
68°E
72°E
76°E
80°E
05 DEC
04 DEC
03 DEC
02 DEC
01 DEC
30 NOV
0.0
-0.2
-0.4
-0.6
-0.8
-1.0
-1.2
-1.4
-1.6
-1.8
-2.0
-2.2
-2.4
-2.6
-2.8
-3.0
b)
SSTA (°C)
0.0
−0.5
−1.0
−1.5
−2.0
−2.5
NOV30
DEC01
DEC02
DEC03
DEC04
DEC05

Figure6.pdf.

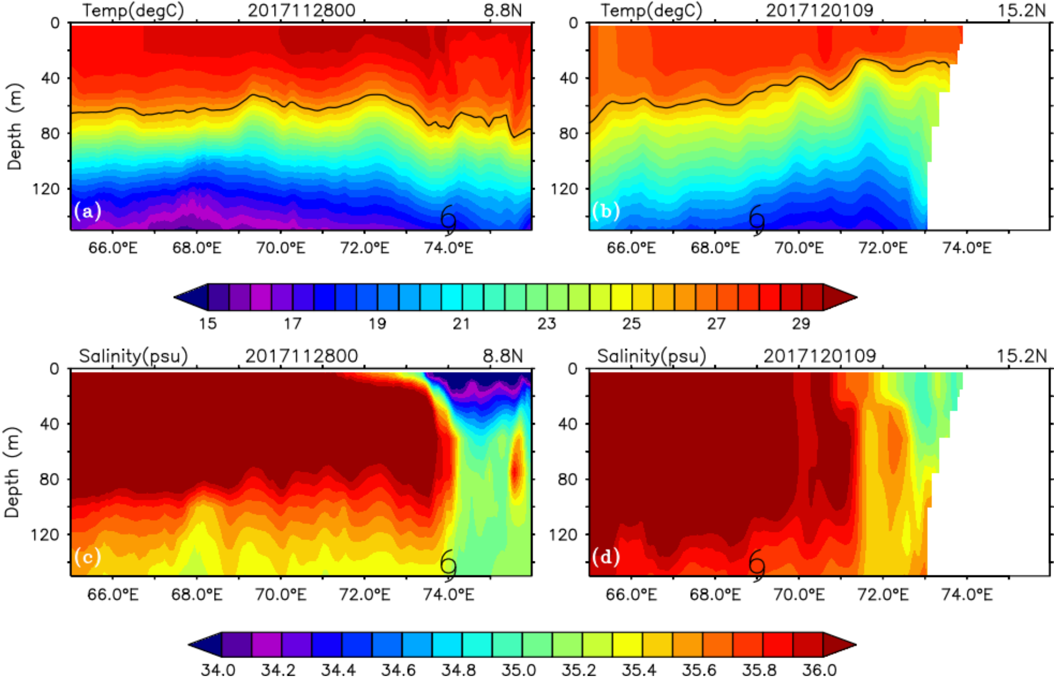

Temp(degC)
2017112800
8.8N
Depth (m)
0
40
80
120
(a)
66.0°E
68.0°E
70.0°E
72.0°E
74.0°E
Temp(degC)
2017120109
15.2N
(b)
15
17
19
21
23
25
27
29
Salinity(psu)
2017112800
8.8N
(c)
Salinity(psu)
2017120109
15.2N
(d)
34.0
34.2
34.4
34.6
34.8
35.0
35.2
35.4
35.6
35.8
36.0

Figure7.pdf.

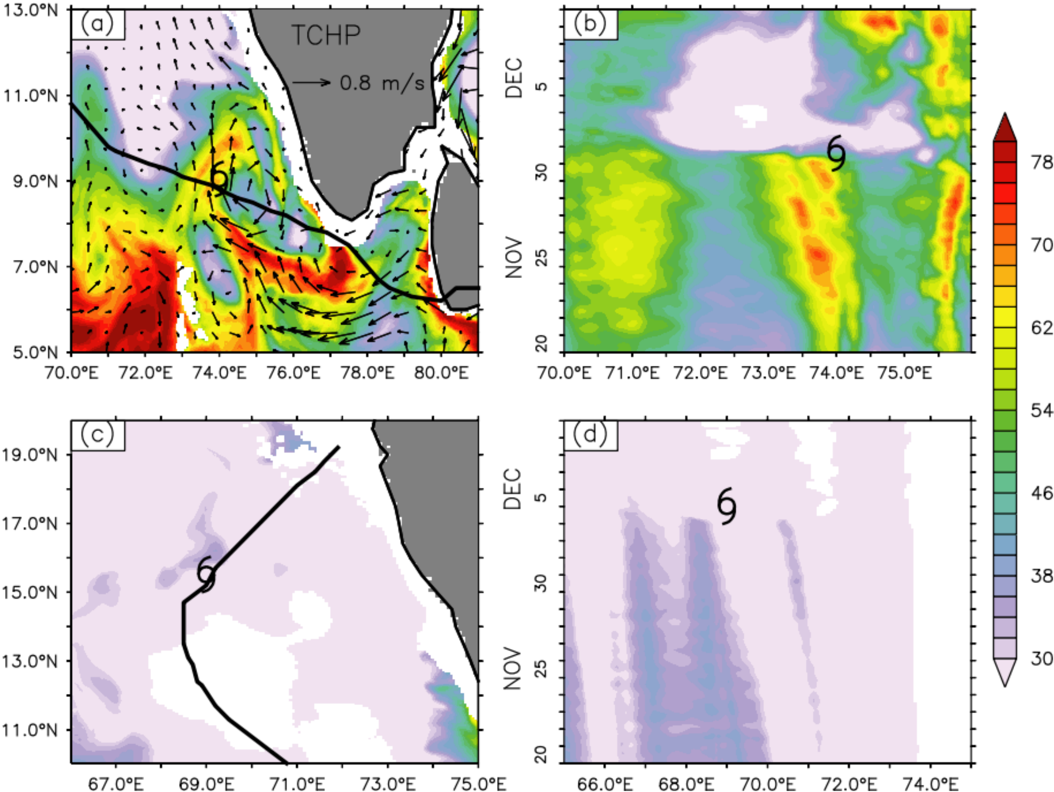

(a)
TCHP
0.8 m/s
13.0°N
11.0°N
9.0°N
7.0°N
5.0°N
70.0°E
72.0°E
74.0°E
76.0°E
78.0°E
80.0°E
(b)
DEC
5
30
NOV
25
20
70.0°E
71.0°E
72.0°E
73.0°E
74.0°E
75.0°E
(c)
19.0°N
17.0°N
15.0°N
13.0°N
11.0°N
67.0°E
69.0°E
71.0°E
73.0°E
75.0°E
(d)
66.0°E
68.0°E
70.0°E
72.0°E
74.0°E
78
70
62
54
46
38
30

Figure8.pdf.

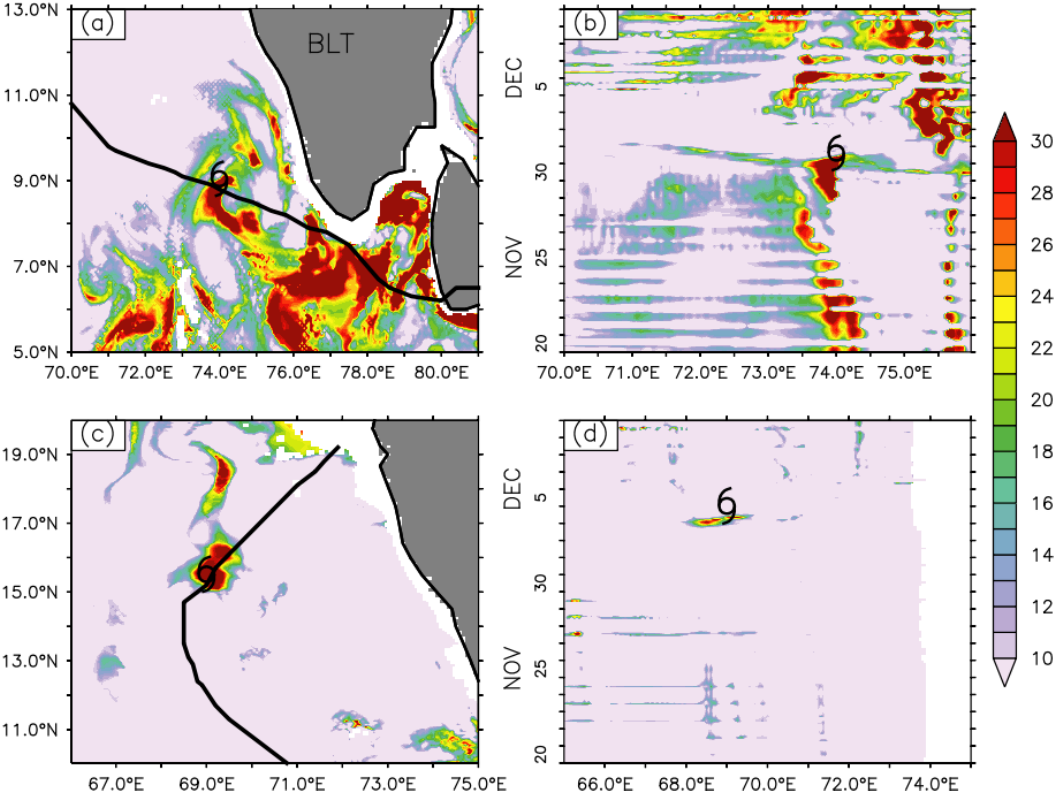

(a)
BLT
13.0°N
11.0°N
9.0°N
7.0°N
5.0°N
70.0°E
72.0°E
74.0°E
76.0°E
78.0°E
80.0°E
(b)
DEC
5
30
NOV
25
20
70.0°E
71.0°E
72.0°E
73.0°E
74.0°E
75.0°E
(c)
19.0°N
17.0°N
15.0°N
13.0°N
11.0°N
67.0°E
69.0°E
71.0°E
73.0°E
75.0°E
(d)
DEC
5
30
NOV
25
20
66.0°E
68.0°E
70.0°E
72.0°E
74.0°E
30
28
26
24
22
20
18
16
14
12
10

Figure9.pdf.

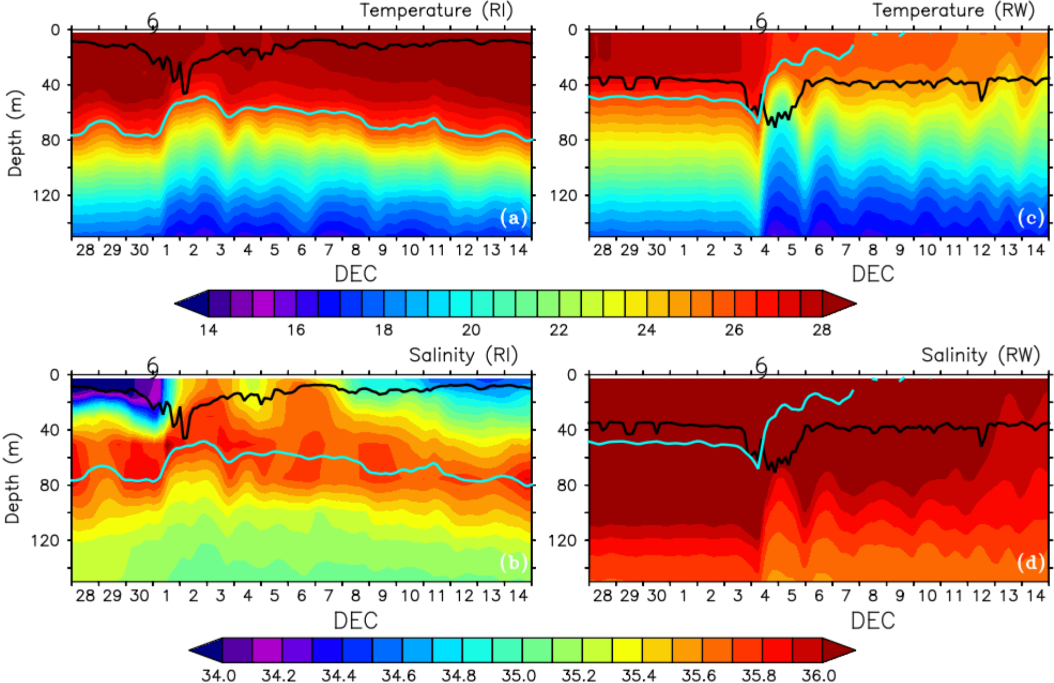

Temperature (RI)
Temperature (RW)
Salinity (RI)
Salinity (RW)
Depth (m)
0
40
80
120
28 29 30 1 2 3 4 5 6 7 8 9 10 11 12 13 14
DEC
(a)
(b)
(c)
(d)
14 16 18 20 22 24 26 28
34.0 34.2 34.4 34.6 34.8 35.0 35.2 35.4 35.6 35.8 36.0

Figure10.pdf.

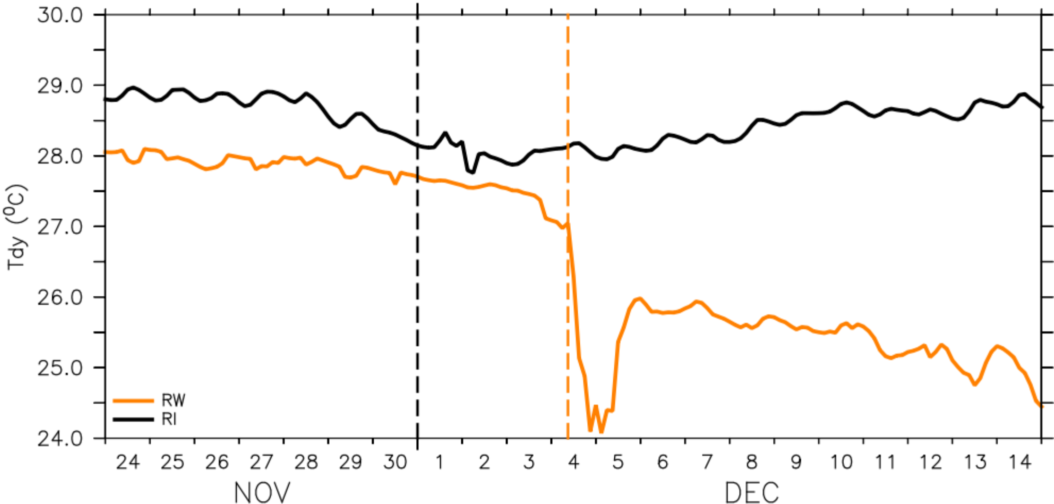

30.0
29.0
28.0
27.0
26.0
25.0
24.0
Tdy (^oC)
RW
RI
24
25
26
27
28
29
30
1
2
3
4
5
6
7
8
9
10
11
12
13
14
NOV
DEC

Figure11.pdf.

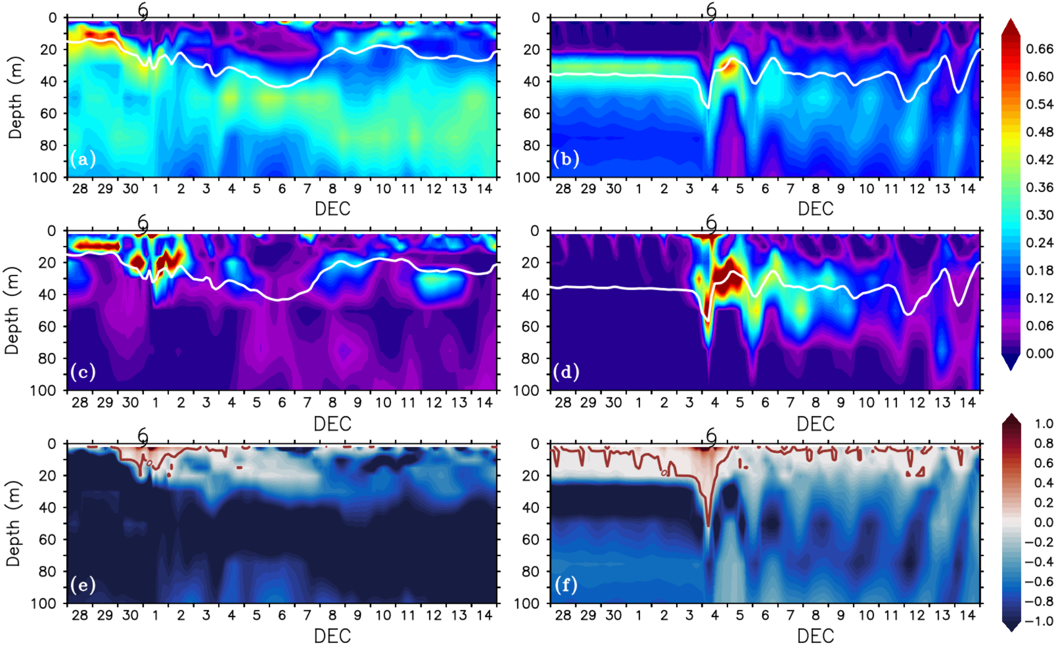

(a)
(b)
(c)
(d)
(e)
(f)
Depth (m)
DEC
0 20 40 60 80 100
28 29 30 1 2 3 4 5 6 7 8 9 10 11 12 13 14
0.66 0.60 0.54 0.48 0.42 0.36 0.30 0.24 0.18 0.12 0.06 0.00
1.0 0.8 0.6 0.4 0.2 0.0 −0.2 −0.4 −0.6 −0.8 −1.0